

1 **A lettuce growth model responding to a broad range of greenhouse climates**

2

3 Weituo Sun ^{a,b}, Anne Coules ^b, Chunjiang Zhao ^{c*}, Chungui Lu ^{b*}

4

5 ^a Intelligent Equipment Research Center, Beijing Academy of Agriculture and Forestry
6 Sciences, Beijing 100097, China

7 ^b School of Animal, Rural and Environmental Sciences, Nottingham Trent University,
8 Nottinghamshire NG25 0QF, UK

9 ^c National Engineering Research Center for Information Technology in Agriculture, Beijing
10 100097, China

11

12

13

14 * Corresponding authors.

15 E-mail address: zhaocj@nercita.org.cn (Chunjiang Zhao); chungui.lu@ntu.ac.uk (Chungui
16 Lu)

17

18 **Abstract**

19

20 Crop models serve as a basis for optimal management of greenhouse climate, while the
21 current simulations for lettuce growth are incomplete. This study presents a lettuce growth
22 model that describes the effects of a broad range of greenhouse climates, including air
23 temperature with extreme conditions, humidity, CO₂ concentration, and shortwave radiation on
24 dynamics of the single state variable, structural crop dry weight. The proposed model
25 framework performs two parallel sets of mass flows: dry matter accumulation and buffer
26 evolution. The buffer carbohydrates flow to growth conversion based on the temperature-
27 dependent sink strength. The inhibition of canopy assimilation occurs when the carbohydrate
28 storage approaches the buffer capacity. The humidity effects are incorporated by describing
29 stomatal resistance and specific leaf area of new leaves. The model was first calibrated at both
30 sub-model and model levels and then validated against data collected in three experiments,
31 covering a broad range of greenhouse climates. Results demonstrated that the model
32 performance was good and acceptable; the simulated crop dry weights closely mirrored the
33 measured values, with the RRMSE of 10.5-24.9% and the RMSE of 0.0070-0.0131 kg m⁻². The
34 model predicted the leaf area index with an RRMSE of 12.1-54.7% and performed well for the
35 vegetative growth stage concerned by commercial production. The photosynthesis inhibition
36 time accounted for 27-41% of the total photosynthesis time, indicating that the model
37 framework and underlying hypothesis worked in simulations. The developed model, simulating
38 instantaneous lettuce dynamics for the potential situation, can be applied to low-tech
39 greenhouses and enables optimal control of all four climate factors.

40

41 **Keywords:** Crop growth model; Lettuce; Greenhouse climate; Dry weight; Leaf area index;
42 Photosynthesis inhibition

43 **Nomenclature**

<i>Symbols</i>	
A_C	gross canopy assimilation rate, $\text{kg (CO}_2\text{) m}^{-2}$ (ground) s^{-1}
A_L	gross assimilation rate of individual leaves, $\text{kg (CO}_2\text{) m}^{-2}$ (leaf) s^{-1}
$A_{L,C}$	gross leaf assimilation rate at a whole canopy level, $\text{kg (CO}_2\text{) m}^{-2}$ (leaf) s^{-1}
$A_{L,c,n}$	net leaf assimilation rate only limited by CO_2 concentration, $\text{kg (CO}_2\text{) m}^{-2}$ (leaf) s^{-1}
A_{L,l_i}	gross leaf assimilation rate at canopy depth l_i , $\text{kg (CO}_2\text{) m}^{-2}$ (leaf) s^{-1}
$A_{L,mm}$	maximum endogenous photosynthetic capacity, representing the theoretical value of the net assimilation rate at both high levels of light and CO_2 , $\text{kg (CO}_2\text{) m}^{-2}$ (leaf) s^{-1}
$A_{L,sat}$	potential gross leaf assimilation rate at light saturation, $\text{kg (CO}_2\text{) m}^{-2}$ (leaf) s^{-1}
$A_{L,sat,n}$	net leaf assimilation rate at light saturation, $\text{kg (CO}_2\text{) m}^{-2}$ (leaf) s^{-1}
C_{buf}	amount of stored carbohydrates in the buffer, $\text{kg (CH}_2\text{O) m}^{-2}$ (ground)
$C_{buf,max}$	maximum buffer capacity for diurnal assimilates storage, $\text{kg (CH}_2\text{O) m}^{-2}$ (ground)
c_H	constant for calculating maximum electron transport rate, J mol^{-1}
$c_{r,I}$	canopy reflection coefficient for shortwave radiation, -
$c_{r,PAR}$	canopy reflection coefficient for PAR, -
$c_{rc,1}$	coefficient of the quadratic term of the fitting for carboxylation resistance description, $\text{m s}^{-1} \text{ } ^\circ\text{C}^{-2}$
$c_{rc,2}$	coefficient of the linear term of the fitting for carboxylation resistance description, $\text{m s}^{-1} \text{ } ^\circ\text{C}^{-1}$

$c_{rc,3}$	constant term of the fitting for carboxylation resistance description, $m s^{-1}$
$c_{Rd,25,r}$	maintenance coefficient for the root at 25°C, $kg (CH_2O) kg (dry matter) s^{-1}$
$c_{Rd,25,sh}$	maintenance coefficient for the shoot (leaf) at 25°C, $kg (CH_2O) kg (dry matter) s^{-1}$
c_S	constant for calculating maximum electron transport rate, $J mol^{-1} K^{-1}$
c_α	factor that converts assimilated CO_2 into sugar equivalents in the photosynthesis process, -
c_β	factor that converts carbohydrates to structural material due to the growth respiration and synthesis, -
c_ζ	scaling factor that accounts for the faster diffusion of H_2O compared to CO_2 in crossing stomata, -
$c_{\sigma,1}$	coefficient 1 for root ratio description, $plants kg^{-1}$
$c_{\sigma,2}$	coefficient 2 for root ratio description, -
$e_{c,a}$	leaf to air vapour pressure difference, Pa
E_J	activation energy of the maximum electron transport rate, $J mol^{-1}$
$e_{s,air}$	saturated vapour pressure of greenhouse air, Pa
$f_{I,s}$	radiation dependency for stomatal resistance, -
$f_{I,SLA}$	factor accounting for the effect of radiation on SLA , -
$f_{Tc,s}$	temperature dependency for stomatal resistance, -
$f_{Xc,s}$	CO_2 dependency for stomatal resistance, -
$f_{Xh,s}$	humidity dependency for stomatal resistance, -
$f_{Xh,SLA}$	factor accounting for the effect of air humidity on SLA , -
h_{buf}	buffer dependent inhibition function for canopy assimilation, -

I	shortwave radiation at the top of the canopy, W m^{-2} (ground)
I_a	absorbed shortwave radiation by the canopy, W m^{-2} (ground)
$I_{a,L,ref}$	arbitrary reference absorbed shortwave radiation by leaves corresponding to SLA_{ref} , W m^{-2} (leaf)
J_{max}	maximum electron transport rate, $\mu\text{mol (e-)} \text{m}^{-2}$ (leaf) s^{-1}
$J_{max,25}$	maximum electron transport rate at 25°C, $\mu\text{mol (e-)} \text{m}^{-2}$ (leaf) s^{-1}
k_I	extinction coefficient for shortwave radiation, -
k_{PAR}	extinction coefficient for PAR, -
LAI	leaf area index, m^2 (leaf) m^{-2} (ground)
Le	Lewis number for CO_2 in air at 25 °C, -
l_f	leaf characteristic dimension, taken as the mean leaf width in wind direction, m
l_i	canopy depth, m^2 (leaf) m^{-2} (ground)
M_{CO_2}	molar mass of CO_2 , kg mol^{-1}
PAR_a	absorbed photosynthetically active radiation (PAR), W m^{-2} (leaf)
$PAR_{a,li}$	absorbed PAR for a specific leaf layer at canopy depth l_i , W m^{-2} (leaf)
$Q_{10,gr}$	Q_{10} factor for crop growth, -
$Q_{10,Rd}$	Q_{10} value for maintenance respiration, -
$Q_{10,\Gamma}$	Q_{10} value for CO_2 compensation point, -
r_b	boundary layer resistance, s m^{-1}
r_c	carboxylation resistance, s m^{-1}
r_{CO_2}	total leaf resistance to CO_2 diffusion, s m^{-1}
R_d	crop maintenance or dark respiration rate, $\text{kg (CH}_2\text{O)} \text{m}^{-2}$ (ground) s^{-1}

$R_{d,25}$	leaf maintenance (dark) respiration rate at a reference temperature of 25 °C, kg (CH ₂ O) m ⁻² (ground) s ⁻¹
R_g	gas constant, J mol ⁻¹ K ⁻¹
RGR_{max}	maximum relative growth rate that depends on temperature, s ⁻¹
$RGR_{max,20}$	maximum relative growth rate of dry matter at 20 °C, s ⁻¹
$r_{H_2O,min}$	minimum possible internal crop resistance to H ₂ O, s m ⁻¹ .
r_s	stomatal resistance, s m ⁻¹
r_t	turbulence resistance, s m ⁻¹
s	slope of smoothing functions
SLA	specific leaf area of new leaves, expressing the amount of leaf area per unit shoot dry matter, m ² (leaf) kg ⁻¹ (leaf)
SLA_{ref}	reference SLA at the reference absorbed shortwave radiation by leaves $I_{a,L,ref}$ and the reference relative humidity $X_{h,ref}$, m ² (leaf) kg ⁻¹ (leaf)
t	time, s
$T_{0,K}$	0°C in Kelvin = 273.15 K
$T_{25,K}$	25°C in Kelvin, = (25 + $T_{0,K}$) K
T_c	canopy temperature, equivalent to air temperature X_t , °C
$T_{c,K}$	canopy temperature in Kelvin, = (T_c + $T_{0,K}$) K
$T_{c,RGR}$	temperature to achieve the saturation relative growth rate, °C
v_a	wind speed inside the greenhouse, m s ⁻¹
X_c	CO ₂ concentration of the indoor air, μmol (CO ₂) mol ⁻¹ (air)
X_d	crop dry weight, kg m ⁻² (ground)
X_h	air relative humidity, -
$X_{h,ref}$	arbitrary relative humidity corresponding to SLA_{ref} , -

X_t	air temperature, °C
z	Auxiliary parameter to ensure differentiability
<i>Greek symbols</i>	
β_l	relative change in <i>SLA</i> per unit change in absorbed shortwave radiation by leaves, $\text{m}^2 \text{ (leaf)} \text{ W}^{-1}$
β_{xh}	relative change in <i>SLA</i> per unit change in relative humidity, -
Γ	CO_2 compensation concentration, $\mu\text{mol} \text{ (CO}_2\text{)} \text{ mol}^{-1} \text{ (air)}$
Γ_{T20}	reference value of the CO_2 compensation point at 20 °C, $\mu\text{mol} \text{ (CO}_2\text{)} \text{ mol}^{-1} \text{ (air)}$
ε	light use efficiency by photorespiration, $\text{kg} \text{ (CO}_2\text{)} \text{ J}^{-1} \text{ (absorbed)}$
ε_0	light use efficiency at very high CO_2 concentration in the absence of photorespiration, $\text{kg} \text{ (CO}_2\text{)} \text{ J}^{-1} \text{ (absorbed)}$
ρ_c	plant density, $\text{plants m}^{-2} \text{ (ground)}$
ρ_{CO_2}	CO_2 density, kg m^{-3}
$\rho_{\text{CO}_2,0}$	CO_2 density at temperature of $T_{0,K}$, kg m^{-3}
σ_{buf}	ratio of the maximum buffer capacity to crop dry weight, -
σ_{PAR}	ratio of PAR to shortwave radiation, -
σ_r	ratio of the root dry weight to the crop dry weight, -
<i>Abbreviations</i>	
CSG	Chinese solar greenhouse
Exp_c	the calibration experiment
Exp_v1	the first validation experiment
Exp_v2	the second validation experiment
PAR	photosynthetically active radiation

RMSE	root mean square error
RRMSE	relative root mean square error
SLA	specific leaf area
VPD	vapour pressure deficit

44

45

46 **1. Introduction**

47 The primary objective of greenhouse climate control is to improve the economic
48 performance of the greenhouse crop production process. Conventional control schemes based
49 on heuristic rules have limited success in maximising the net revenue of greenhouse cultivation
50 (van Straten, van Willigenburg, van Henten, & van Ooteghem, 2010). Optimal control, which
51 explicitly balances the benefits of the marketable product against the operating costs of the
52 climate conditioning equipment, offers a promising method to realise a higher production
53 efficiency (Chalabi, Biro, Bailey, Aikman, & Cockshull, 2002; Ioslovich, 2009; Tap, 2000; van
54 Beveren, Bontsema, van Straten, & van Henten, 2015). Using a model-based control
55 mechanism, the performance of an optimal climate control system for greenhouse crop
56 production largely depends on the accuracy of its underlying process model, although control
57 algorithms, such as receding horizon (Kuijpers, Antunes, van Mourik, van Henten, & van de
58 Molengraft, 2022), can address model uncertainties and improve system robustness to some
59 extent. To apply optimal control theory in practice, the system model must accurately predict
60 greenhouse climate-crop growth dynamics affected by control adjustments and weather
61 disturbances, based on which the optimal control problem solving can link energy consumption
62 with crop revenue to seek optimised control trajectories. Due to the complexity of the entire
63 process description, the system model formulation typically integrates both a greenhouse
64 climate model and a crop growth model (Tap, 2000; van Henten, 1994a), with the latter often
65 presenting more significant challenges (van Straten, Challa, & Buwalda, 2000). The lettuce is
66 one of the most important horticultural crops. To generate an efficient optimal control system
67 for climate management of greenhouses cultivating lettuce, an accurate lettuce growth model
68 with robust generalisation is essential. Theoretically, the lettuce growth model should describe
69 the complete effects of greenhouse climate variables. In particular, shortwave radiation, CO₂
70 concentration, air temperature and humidity (Stanghellini, van't Oosfer, & Heuvelink, 2019).

71 As reviewed by van Holsteijn (1980), the quantitative analysis of growth for lettuce dates
72 back to the 1960s, providing valuable insights for subsequent modelling work. Current lettuce
73 growth models can be generally distinguished according to two levels of production situation:
74 potential production and nitrogen-limited production. Seginer, Buwalda, and van Straten (1999)
75 developed a lettuce model with two compartments (structure and vacuole) to simulate lettuce
76 growth and nitrate content under limited nitrogen supply. This model was derived from their
77 previous model for potential production (Seginer, van Straten, & Buwalda, 1998) by
78 introducing a nitrogen balance of the vacuoles and was subsequently modified to cover severe
79 nitrogen-stress scenarios by extending a storage compartment for excess carbon (Seginer, 2003).
80 Its parameterisation was later optimised based on sensitivity and correlation analysis by
81 Ioslovich, Moran, and Gutman (2005). The above ‘Nicolet’ model, which describes the effects
82 of indoor air temperature, CO₂ concentration, and light, as well as nitrogen in the nutrient
83 solution, can serve as the basis for greenhouse climate and nutrient controls to prevent excessive
84 nitrate content in crops (Seginer, Linker, Buwalda, van Straten, & Bleyaert, 2003), as well as
85 for rapid fault detection in hydroponic systems (Mathieu et al., 2006). However, optimal climate
86 control requires the crop model to describe the potential production where water and nutrients
87 are adequately provided, and only meteorological conditions determine the growth rate
88 (Goudriaan & van Laar, 1994).

89 Several models are available in the literature for dynamic numerical simulation of potential
90 lettuce growth. Early lettuce models were primarily empirical, using logistic, Gompertz, and
91 other sigmoidal forms (Shimizu, Kushida, & Fujinuma, 2008; Stützel & Chen, 2020; Tei,
92 Aikman, & Scaife, 1996), and have continued to attract research attention over the last decade
93 (Carini et al., 2019; Li, Gao, Zhang, Ni, & Mao, 2022). These simple statistical models struggle
94 to explicitly account for the effects of greenhouse climate dynamics. With advances in artificial
95 intelligence, more sophisticated data-driven models represented by neural networks have been

96 developed for lettuce growth simulation. Their effectiveness and feasibility in simulating crop
97 growth, yield, and physiological factors have been demonstrated (Chang, Chung, Fu, & Huang,
98 2021; Mohmed et al., 2023; Mokhtar et al., 2022). However, achieving high prediction accuracy
99 and robust generalisation for practical applications requires vast amounts of data for model
100 training, which presents a significant challenge as it often relies on obtaining crop growth
101 indicators through destructive sampling.

102 Currently, mainstream lettuce growth models are mechanistic, the most commonly used in
103 formulating control systems (Rohde & Forni, 2023; Seginer, Shina, Albright, & Marsh, 1991;
104 van Henten, 1994a; D. Xu, S. Du, & van Willigenburg, 2018; Xu, Du, & van Willigenburg,
105 2019). Mechanistic crop models are expected to generalise better than data-driven models since
106 their development specifically describes processes that influence the state dynamics based on
107 physical, chemical, and biological principles. To generate and solve analytical relationships for
108 CO₂ concentration optimisation in commercial greenhouse lettuce production, Critten (1991)
109 modified an early mechanistic lettuce growth model by (Sweeney, Hand, Slack, & Thornley,
110 1981), which originally included structural and storage dry weights as state variables, to a
111 simplified model with one state by assuming the two weights to be equal. They mainly explain
112 the effects of horizontal radiation and CO₂ concentration. The original model was later
113 optimised to more sensitively incorporate instantaneous and long-term effects of temperature
114 dynamics on photosynthesis and was extensively validated by Pearson, Wheeler, Hadley, and
115 Wheldon (1997). van Henten (1994a) developed both one-state and two-state lettuce growth
116 models for optimal greenhouse climate management. The one-state model uses structural dry
117 weight as the single state variable, assuming that carbohydrates produced by photosynthesis are
118 partly consumed by maintenance respiration, with the remainder used for growth. In contrast,
119 the two-state model (van Henten, 1994b) considers total dry weight as comprising structural
120 and non-structural dry weights. The growth of structural dry matter derives from the

121 transformation of non-structural materials into structural components, with its rate dependent
122 on temperature and the non-structural material proportion. Both models predict the crop dry
123 weight and leaf area index responding to greenhouse climate attributes, including shortwave
124 radiation, CO₂ concentration, and air temperature within a limited range of 5-40 °C. The Eldert
125 lettuce models have been applied in optimal control studies (van Henten, 1994a; van Straten et
126 al., 2010; D. Xu, S. Du, & L. G. van Willigenburg, 2018) and adapted as a TRNSYS component
127 for energy analysis (Talbot & Monfet, 2024). In addition, models based on the framework for
128 potential growth can extend to describe nitrogen accumulation in crops using the turgor
129 maintenance hypothesis (Seginer et al., 1998; K. Zhang, Burns, Broadley, & Turner, 2003),
130 which also fall within the scope of those supporting optimal climate control. Despite their strong
131 generalisation ability and reported good performance, existing process-based lettuce growth
132 models, which hold potential as a basis for optimal greenhouse climate control, are incomplete
133 and lack sufficient motivation for complex control scenarios, thus constraining their practical
134 applicability.

135 The first limitation of current lettuce models is the lack of describing the impact of air
136 humidity on growth. Humidity is an important physical aspect of the greenhouse air that the
137 crop releases water vapour via transpiration. It affects biochemical and morphogenetic
138 processes, such as stomatal conductance, leaf cell elongation, and nutrient absorption (Bakker,
139 1991; Collier & Tibbitts, 1984; Monteith, 1995; X. Zhang et al., 2020). The sensitivity of crop
140 growth to humidity levels is crop species dependent (Mortensen, 1986; Rawson, Begg, &
141 Woodward, 1977). But in general, crop growth is inhibited by extreme humidity situations (very
142 high or low humidity). Hence, including the effects of humidity in the crop growth model has
143 considerable potential to improve model accuracy. With such a model, the optimal control
144 strategies and humidity trajectories will be computed by trade-off additionally concerning the
145 effects of control actions on crop growth induced by humidity changes, leading to a control

146 approach that is much closer to the actual optimum. In contrast, with a model excluding
147 humidity effects, the humidity trajectories will be determined by setpoints and subject to control
148 of other climate variables. For instance, van Henten (1994a) and Tap (2000) accomplished
149 humidity control by requiring the greenhouse relative humidity to stay between a lower and an
150 upper limit, assuming that humidity does not affect crop production between these limits. A
151 sensitivity analysis of the optimal control problem revealed that humidity control strongly
152 influences greenhouse climate control performance, highlighting the need for a detailed
153 description of humidity effects on crop growth (van Henten, 2003).

154 Secondly, current lettuce growth models are primarily developed for typical greenhouse
155 climate conditions. They cannot comprehensively account for the adverse effects of extreme
156 temperatures, especially lacking a robust mechanism to fully describe growth inhibition beyond
157 impacts on leaf photosynthesis, have not been tested under these extreme conditions, or even
158 do not allow for such inputs. For instance, an extremely low night temperature benefits dry
159 matter accumulation in their simulations due to the low consumption of maintenance respiration
160 but inhibits the actual crop growth. Consequently, the optimal control system, in the absence of
161 state constraints, might excessively reduce nighttime temperatures inside the greenhouse,
162 potentially undermining efforts to enhance production efficiency. There is no doubt that crop
163 growth will be inhibited by non-optimal temperature levels (Thompson, Langhans, Both, &
164 Albright, 1998; van Ploeg & Heuvelink, 2005; Volente, 2022). However, temperature
165 fluctuations are allowed in greenhouse climate control to save energy and obtain higher net
166 revenue (Körner & van Straten, 2008; Stanghellini et al., 2019). Furthermore, extreme
167 temperatures frequently occur inside greenhouses with low-tech climate conditioning devices,
168 such as the Chinese solar greenhouse (CSG) (Sun et al., 2015). Therefore, the crop model must
169 also adequately describe the relevant crop processes to a wide range of greenhouse air
170 temperatures.

171 In addition, mechanistic crop models that describe dry matter accumulation based on the
172 differences between photosynthesis and respiration often face challenges in effectively
173 simulating the early stages of crop growth that are sink-limited. As stated by Tei et al. (1996),
174 no successful attempt was made to explain how sink demand can limit growth. This issue still
175 exists in modelling lettuce growth. Lastly, present lettuce models are established at the canopy
176 level, with growth measured by biomass accumulation per unit ground area. However, the
177 specific area for determining the default plant density has not been disclosed. The impact of
178 plant density on model development will be reflected at least in model calibration. Since crop
179 cultivation cannot occupy the entire greenhouse ground due to space needed for walkways,
180 operations, and equipment, it is critical for the practical optimal control to measure the effective
181 cultivation area, focusing on upper limits, and to ensure that the crop model component implies
182 the effective cultivated area-based plant density.

183 In summary, to efficiently deploy optimal control in greenhouse climate management, a
184 mechanistic lettuce growth model that completely describes the effects of greenhouse climate
185 dynamics, particularly with respect to humidity and extreme temperatures, is currently
186 unavailable. Therefore, this study aims to describe, calibrate, and validate such a lettuce growth
187 model that responds to a broad range of greenhouse climates, including shortwave radiation,
188 CO₂ concentration, air temperature with extreme conditions, and air humidity. The developed
189 model is expected to have sufficient accuracy and robust generalisation. The focus is on the
190 shoot environment, and it is assumed that water and nutrients are readily available. Pests,
191 diseases, and weeds are not considered. The model consists of a set of first-order differential
192 equations and simulates instantaneous dynamics of crop growth to facilitate the link with
193 existing greenhouse climate models and its integration into optimal control methods. The main
194 contributions and innovations are as follows:

- 195 • Proposing a novel model framework that performs dry matter accumulation and buffer

196 evolution in parallel, along with the underlying hypothesis of virtual buffer flows and
197 canopy photosynthesis inhibition, by which effects of air temperature, including extreme
198 conditions, on crop growth are adequately described, and sink-limited early growth stages
199 can be effectively simulated.

- 200 • Extending the description of humidity effects regarding stomatal resistance and the
201 specific leaf area (SLA) of new leaves.
- 202 • Simplifying expressions of leaf carboxylation resistance and root ratio by fitting, and
203 imposing constraints on the maximum ground area occupied by a single plant for the
204 implicit plant density.
- 205 • Performing three field experiments, which cover a broad range of greenhouse climates, to
206 calibrate and evaluate the model, as well as analyse the performing mechanism.

207 This study will provide an accurate lettuce growth model with robust generalisation,
208 enabling the formulation of an efficient optimal climate control system for greenhouse lettuce
209 production that covers greenhouses with poor climate conditioning performance, ultimately
210 improving production efficiency through decision support or online control.

211

212 **2. Materials and Methods**

213 **2.1. Experiment design**

214 To obtain data for model calibration and validation, three experiments of greenhouse lettuce
215 cultivation were carried out in CSGs from 9 April to 14 May 2020, from 24 November 2020 to
216 18 January 2021, and from 25 January to 16 March 2022. The three experiment periods were
217 in warm, cold, and cold-warm seasons, enabling the collected greenhouse climate cover from
218 extremely low to extremely high temperatures. The experiment performed in the cold season
219 was used for global calibration and named the calibration experiment (Exp_c) below. The other

220 two in warm and cold-warm seasons, namely the first validation experiment (Exp_v1) and the
221 second validation experiment (Exp_v2), were used for model validation.

222

223 **2.1.1. Experimental greenhouses**

224 The experimental CSGs were located in Fangshan District, Beijing, China (39.62° N, 115.96°
225 E). They were oriented from east to west, consisting of the north wall, side walls, the north roof,
226 and the south roof made of single-layer plastic film. The south roof had two vents that opened
227 from east to west: one at the bottom and one at the top. It was covered with a thermal blanket
228 at night in cold seasons. No extra climate conditioning equipment was used during the
229 experiments. The CSG in Exp_v1 (Fig. 1a) had a floor area of approximately 585 m², with a
230 width of 7.50 m and a length of 78.0 m. The CSG used for Exp_c (Fig. 1b) and Exp_v2 (Fig.
231 1c) had a floor area of approximately 652 m², with a width of 7.55 m and a length of 86.3 m.
232 The floor of both greenhouses was bare soil.

233 The greenhouse climate during the growing period was controlled manually according to the
234 rules followed in regular CSG horticulture practice. Supply of water and fertiliser was also in
235 line with the growers' experience with the control objective of being most beneficial to crop
236 growth. Note that the model uses only environmental factors as external inputs, and it is
237 assumed that water and fertiliser levels were adequate in the experiments.

238



239

240

241 Fig. 1 Experimental greenhouses and lettuce cultivation. a: the first validation experiment; b:
242 the calibration experiment; c: the second validation experiment.

243

244 **2.1.2. Lettuce planting**

245 The lettuce cultivar selected for the experiments was Tiberius RZ (41-27) (produced by Rijk
246 Zwaan, The Netherlands), which is increasingly used for greenhouse lettuce production in
247 China. Lettuce plants were sown and raised in the nursery substrate inside a seedling
248 greenhouse. Then, they were transplanted to soil inside CSGs.

249 In Exp_v1, the lettuce seedlings were transplanted when they had 10 main leaves. The plants
250 were cultivated in east-west rows (Fig. 1a), which occupied parts of the greenhouse floor area
251 with a length of 72.6 m and total width of 3.60 m. There were 255 plants per row, so the row
252 density was 3.51 plants m⁻¹. There were 12 rows and 3060 plants in the greenhouse, that is,
253 11.71 plants m⁻² (ground). In this study, the developed model is oriented to lettuce cultivation
254 with an effective cultivated area-based, instead of an arbitrary ground area-based, plant density.
255 This makes the model practical and universal. The unit ground area on which the simulated
256 crop dry weight and other states are based is the effective cultivated area. This effective area
257 depends on the upper limit of ground area occupied by a single plant. Considering the lettuce's
258 genetic characteristics and harvesting size for commercial purposes, the model limits the
259 maximum ground area occupied by a single lettuce to 0.32×0.32 m square centred on the
260 planting site. This limitation works in dividing the boundary of an effective cultivated area and
261 preventing the density from being too low. If not, the model will easily overestimate crop
262 growth and lose its universality. This is because, like most other models, this model assumes
263 that the canopy infinitely spreads in the selected ground area. However, many blank areas exist
264 outside the cultivation area and even between plants inside the greenhouse. The model global
265 calibration below contributes to the implicit plant density of the model.

266 In Exp_c, the lettuce seedlings were transplanted when they had 4 main leaves. The plants
267 were cultivated in east-west rows (Fig. 1b), and the cultivated area had a length of 78.1 m and
268 total width of 4.50 m. There were 265 plants per row, so the row density was 3.39 plants m⁻¹.
269 There were 15 rows and 3975 plants in the greenhouse, and the plant density was 11.31 plants
270 m⁻² (ground). In Exp_v2, the lettuce seedlings were transplanted when they had 5 main leaves.
271 The plants were cultivated in north-south ridges, with 4 rows of crops on each ridge (Fig. 1c).
272 The cultivated area had a total length of 59.0 m and a width of 6.25 m. There were 18 plants
273 per row; thus, the row density was 2.88 plants m⁻¹. There were 236 rows and 4248 plants in the
274 greenhouse, that is 11.52 plants m⁻² (ground).

275

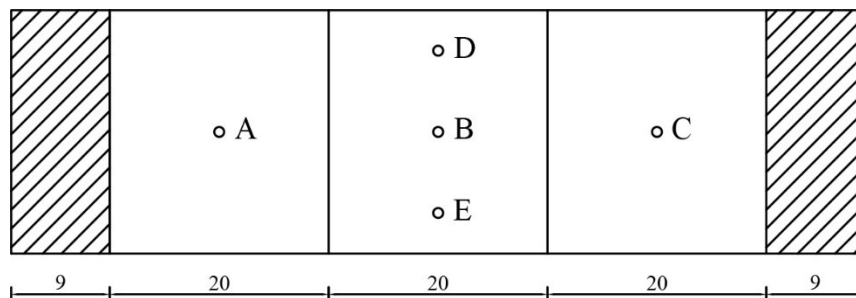
276 **2.1.3. Data collection**

277 During the three experiments, crop growth indicators and greenhouse climate measurements
278 were recorded. To ensure uniform data, buffer zones were set factitiously to mitigate the effects
279 of CSG side walls and the entrance door on indoor climate and lettuce growth. The remaining
280 was the sampling zone, where the lettuce samplings and climate measurements were performed
281 (Fig. 2). For destructive crop measurements, the sampling zone was divided into 3 blocks, and
282 an equal number of plants were randomly selected for harvest from each block to account for
283 the effect of greenhouse climate gradients. Throughout the growing season, samples were
284 collected every 5 days in the three experiments: 18 plants in Exp_v1 and Exp_c, and 6 plants
285 in Exp_v2. One exception was the first sampling; the samples were the seedlings for
286 transplanting, and 6 plants were sampled given the uniform nursery climate. Dry weights of
287 both root and shoot, leaf area, canopy diameter, and other growth indicators were determined
288 for each plant. Dry weight was obtained after oven drying at 105°C for 30 min and then 70 °C
289 until the samples had constant weight, and it was measured by an analytical balance (accuracy:

290 0.001 g). Leaf area was measured by a portable leaf area meter (LI-3000C, USA, accuracy:
291 within $\pm 2\%$ for samples $>50 \text{ cm}^2$).

292 Greenhouse climate includes solar radiation (shortwave radiation), air temperature, relative
293 humidity, and CO_2 concentration at a height of 1.5 m above the CSG ground. Of which, air
294 temperature, relative humidity and CO_2 were measured and recorded by a portable data logger
295 (ESPEC THCO2, Japan, accuracy: $\text{CO}_2 \pm 50 \mu\text{mol mol}^{-1}$) using sensors (RSH-3020, Japan,
296 accuracy: temperature $\pm 0.3 \text{ }^\circ\text{C}$, relative humidity $\pm 2.5\%$) with radiation shielding. Solar
297 radiation was measured by pyranometers (Kipp&Zonen CMP6, The Netherlands, sensitivity:
298 $5\text{-}20 \mu\text{V/W/m}^2$) and recorded by Campbell CR1000 (USA) data logger. Climatic data was
299 recorded with a time step of 5 minutes. The specific layout of climate measurement points is
300 shown in Fig. 2.

301



302

303 Fig. 2 Lettuce sampling area and layout of climate measurement points (unit: m, taking the
304 first validation experiment for example). Measurement points of temperature, humidity and
305 CO_2 are located at A-E points. Measurement points of shortwave radiation are located at A-C
306 points. Shadow areas denote buffer zones where lettuce is cultivated but not sampled. The
307 model study uses the average values of these measuring points and samples.

308 In Exp_v1, performed in the warm season, the roof and side vents were almost always open,
309 resulting in good ventilation and a relatively uniform climate inside the greenhouse. At the same
310 time, lettuce cultivation had a great demand for irrigation in high temperatures. Due to the east-
311 west cultivation pattern, in which the drip irrigation belt extended a long distance of half the

312 CSG length, insufficient irrigation for some plants might occur. Therefore, the top 12 of the 18
 313 lettuce samples in crop dry weight were selected for model study to avoid potential water and
 314 fertiliser stress. In Exp_c and Exp_v2, seedlings were transplanted in the cold season, and the
 315 recovering period lasted for several days. In order to ensure that the data used for model
 316 calibration and validation were representative, the measurements of the second sampling
 317 performed on the fifth day from the transplanting date (Day 0) were selected as the initial states
 318 of model simulations. As to the analysis above, the initial crop states used for model simulations
 319 are listed in Table 1.

320

321 Table 1 Initial crop states used for the lettuce growth model simulations.

Experiment number	Plant density [plants m ⁻²]	Initial crop	Initial crop	Initial leaf	Initial buffer	
		dry weight of individual plant [g/plant]	dry weight [kg m ⁻² (ground)]	area of individual plant [cm ² /plant]	Initial leaf area index [-]	storage [kg (CH ₂ O) m ⁻² (ground)]
Exp_v1	11.71	0.3889	4.5538×10 ⁻³	146.47	0.1715	0
Exp_c	11.31	0.1112	1.2578×10 ⁻³	37.63	0.0426	0
Exp_v2	11.52	0.1716	1.9766×10 ⁻³	86.50	0.0996	0

322

323

324 2.2. Model description

325

326 2.2.1. Model overview

327

328 The lettuce growth model is essentially based on earlier crop growth models (Goudriaan &
 329 van Laar, 1994; Spitters, van Keulen, & van Kraalingen, 1989; van Henten, 1994a; van
 330 Ooteghem, 2010). It was extended with a temperature-dependent growth inhibition function on

331 the basis of buffer evolution, achieved by the new crop model framework (Fig. 3), and a set of
332 humidity-related equations.

333

334 The state of the lettuce crop is described by a single state variable, structural dry weight, that
335 is, the crop dry weight. The model describes the effects of a broad range of greenhouse climates,
336 including air temperature with extreme conditions, humidity, CO₂ concentration, and shortwave
337 radiation on lettuce growth. The model simulates instantaneous crop growth on a time scale of
338 one second, requiring model inputs to be in time series marked in seconds but allowing for input
339 data of different time intervals.

340

341 The proposed model framework performs two parallel sets of mass flows: dry matter
342 accumulation and buffer evolution. The model assumes that the lettuce has a virtual
343 carbohydrate (CH₂O) buffer, also namely assimilate pool, temporarily storing assimilate. The
344 buffer affects crop photosynthesis through the diurnal courses of its carbohydrate storage.
345 Unlike most other crop models, this buffer does not participate in dry matter formation as a dry
346 matter component. Instead, it is only used for regulating photosynthesis.

347

348 The processes for dry matter accumulation are as follows. The carbohydrates produced by
349 canopy photosynthesis are partly consumed in maintenance respiration. The remaining
350 carbohydrates are converted into structural material and partitioned among various plant organs.
351 In conversion, part of the weight is lost by growth respiration.

352

353 The rate of canopy photosynthesis serves as a basis for dry matter accumulation. It is
354 calculated by integrating assimilation rates over the canopy leaf layers obtained through the
355 photosynthesis-light response of individual leaves. That rate depends mainly on the radiant

356 energy absorbed by the canopy, canopy temperature, CO₂ concentration and air humidity inside
357 the greenhouse. Since the lettuce model is supposed to work in extreme climate conditions
358 where the constant leaf resistances to CO₂ diffusion do not apply, a model including the
359 humidity effect is used to compute the stomatal resistance. For leaf morphogenesis, the SLA of
360 new leaves is defined in relation to climate factors that include humidity and radiation.

361

362 The processes for buffer evolution are as follows. The buffer receives carbohydrates
363 produced by canopy photosynthesis. Simultaneously, the carbohydrates stored in the buffer
364 flow to maintenance respiration and the process of growth conversion or partitioning. The
365 partitioning of the produced dry matter is determined by the maximum growth rate (sink
366 strength) of organs or the whole crop. That is the maximum growth rate of the whole crop
367 described by a function of instantaneous temperature calls for an equal buffer flow rate towards
368 the conversion process. As adverse air temperatures, both during the day and night, inhibit the
369 partitioning, the carbohydrate flows distributed from the buffer to the conversion process are
370 accordingly reduced. Then, the carbohydrate amount in the buffer is more likely to reach high
371 levels during daytime photosynthesis. The photosynthesis rate is inhibited when the
372 carbohydrate amount reaches the maximum storage capacity of the buffer. The effects of
373 extreme temperatures, beyond their instantaneous impact on photosynthesis, were incorporated
374 into the model by describing the above hypothesis of buffer flows and photosynthesis inhibition.

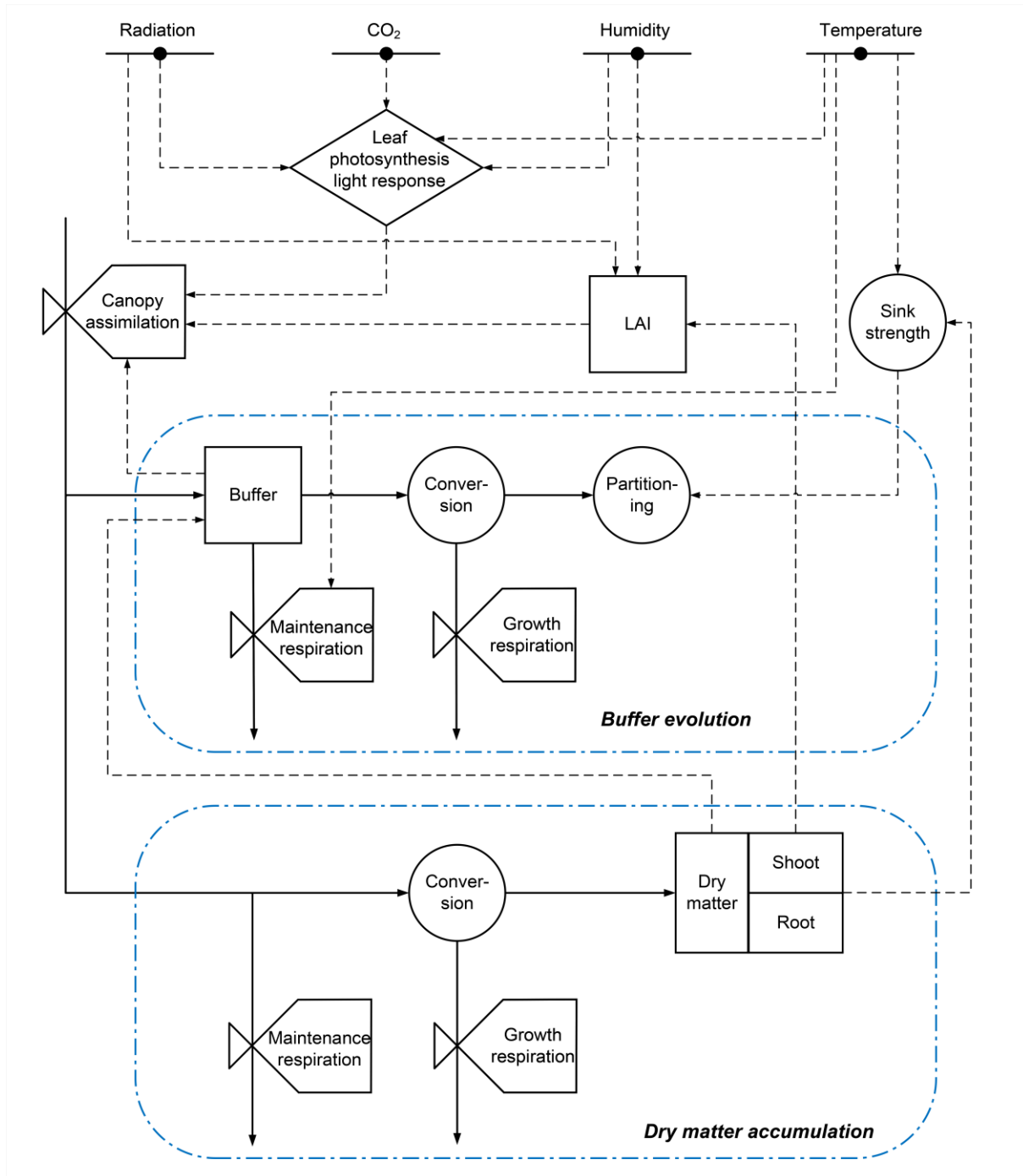
375

376 For simplicity, the root ratio is described as a descriptive logarithmic function of the
377 individual plant dry weight. Also, a descriptive function fitted from complex equations
378 describes the leaf carboxylation resistance, enabling the model to allow temperature inputs in
379 large ranges.

380

381 The two parallel sets of mass flows share paths but differ in logic. In dry matter accumulation,
 382 there is no restriction on the mass flow to growth conversion after photosynthesis. However, in
 383 buffer evolution with virtual mass flows, the mass flow to growth conversion performs the
 384 potential growth rate of the crop.

385



386

387 Fig. 3 Schematic diagram of the lettuce growth model using a modelling formalism of
 388 Forrester. The boxes are state variables of the model, valves are rate variables, circles are
 389 auxiliary variables, and the straight lines crossing solid circles represent input variables. The
 390 dashed lines represent information flows, and the solid lines represent mass flows.

391

392 2.2.2. Model equations

393

394 *Dry matter production*

395

396 In line with the crop growth formulation by SUCROS1 (Goudriaan & van Laar, 1994; van
 397 Laar, Goudriaan, & van Keulen, 1997) and the one-state variable lettuce growth model (van
 398 Henten, 1994a), the basis for calculating dry matter production is the net CO₂ assimilation rate
 399 of the canopy. A buffer-related inhibition function is introduced to deal with particular growth
 400 cases caused by extreme climate conditions. This gives rise to the following description of the
 401 dry matter production,

402

$$\frac{dX_d}{dt} = c_\beta \cdot (c_\alpha \cdot A_C \cdot h_{buf} - R_d) \quad (1)$$

403

404 where X_d [kg m⁻² (ground)] is the crop dry weight, A_C [kg (CO₂) m⁻² (ground) s⁻¹] is the gross
 405 canopy assimilation rate, R_d [kg (CH₂O) m⁻² (ground) s⁻¹] is the crop maintenance respiration
 406 rate, c_β [-] is the factor converts carbohydrates to structural material due to the growth
 407 respiration and synthesis, c_α [-] is the factor converts assimilated CO₂ into sugar equivalents in
 408 the photosynthesis process, h_{buf} [-] is the buffer dependent inhibition function for canopy
 409 assimilation, t [s] is the time. Eq. (1) asserts that the assimilates give priority to maintenance
 410 respiration. Then, all the remaining assimilates are used for structural dry matter production. In

411 this model and most other crop growth models, A_C has already subtracted photorespiration
 412 consumption, which is the so-called apparent gross assimilation rate. Accordingly, the net
 413 assimilation rate means the gross assimilation rate minus the maintenance respiration rate.

414

415 *Assimilation inhibition*

416

417 The buffer storage status affects canopy photosynthesis. This model assumes that when the
 418 carbohydrate storage approaches the maximum buffer capacity, further carbohydrates cannot
 419 be stored, and photosynthesis will be inhibited. In this case, the canopy assimilation does not
 420 stop but offsets the instantaneous carbohydrate consumption for biomass maintenance and
 421 potential crop growth. The buffer dependent inhibition function h_{buf} [-] is described by

422

$$h_{buf} = \begin{cases} 1, & C_{buf} < C_{buf,max} \\ \min\left(\frac{R_d + \frac{RGR_{max} \cdot X_d}{c_\beta}}{c_\alpha \cdot A_C}, 1\right), & C_{buf} = C_{buf,max} \quad (A_C \neq 0) \end{cases} \quad (2)$$

423

424 A two-state variable crop growth model supposes that plant dry matter can be divided into
 425 structure and storage. The rate of structural growth depends on the amount of storage substrate
 426 present (Thornley & Hurd, 1974). Our model assumes the lettuce crop only has structural dry
 427 matter. In the line of dry matter accumulation, there is no restriction on the mass flow to growth
 428 conversion after photosynthesis. While in the other parallel line of buffer evolution, whenever
 429 the carbohydrates in the buffer are available, they flow to growth conversion based on the
 430 maximum growth rate (sink strength). In other words, the structural growth rate in buffer design
 431 is sink determined. The maximum relative growth rate RGR_{max} [s^{-1}] is adapted from (van Henten,
 432 1994b)

433

$$RGR_{max} = \begin{cases} RGR_{max,20} \cdot Q_{10,gr}^{\frac{T_c-20}{10}}, T_c \leq T_{c,RGR} \\ RGR_{max,20} \cdot Q_{10,gr}^{-\frac{T_c-20}{10}}, T_c > T_{c,RGR} \end{cases} \quad (3)$$

434

435 Vanthoor (2011) set the maximum buffer capacity to a fixed value of 20×10^{-3} kg (CH₂O) m⁻²
 436 (ground), assuming that it is equal to the sum of carbohydrates produced at potential
 437 photosynthesis on a daily basis. However, a biomass-varying storage capacity is needed to
 438 realise the inhibition function of the buffer. According to Goudriaan, van Laar, van Keulen, and
 439 Louwse (1985), if the plant does not have sufficient sinks, a buffer storage level rising above
 440 20% on a dry weight basis will gradually diminish the carboxylation conductance and
 441 assimilation rate. So, in this model, the maximum buffer capacity $C_{buf,max}$ [kg (CH₂O) m⁻²
 442 (ground)] is assumed as

443

$$C_{buf,max} = \sigma_{buf} \cdot X_d \quad (4)$$

444

445 The evolution of stored carbohydrates in the buffer is determined by carbohydrate flow from
 446 actual photosynthesis as well as flows to maintenance respiration and growth conversion
 447 processes. These flows do not contribute to an empty buffer unless they can increase the buffer
 448 storage. The variation of the amount of stored carbohydrates in the buffer C_{buf} [kg (CH₂O) m⁻²
 449 (ground)] is described by

450

$$\frac{dC_{buf}}{dt} = c_\alpha \cdot A_C \cdot h_{buf} - R_d - \frac{RGR_{max} \cdot X_d}{c_\beta}, 0 \leq C_{buf} \leq C_{buf,max} \quad (5)$$

451

452 ***Canopy Assimilation***

453

454 The gross canopy assimilation rate A_C [$\text{kg}(\text{CO}_2) \text{m}^{-2}(\text{ground}) \text{s}^{-1}$] is described by

455

$$A_C = A_{L,C} \cdot LAI \quad (6)$$

456

457 $A_{L,C}$ is obtained from the weighted average assimilate rate over the horizontal leaf layers of
458 the canopy. This is achieved using a three-point Gaussian integration (Goudriaan, 1986). The
459 cumulative LAI at each leaf layer is used to express the canopy depth l_i [$\text{m}^2(\text{leaf}) \text{m}^{-2}(\text{ground})$]
460 that locates leaf layers. From top to bottom, the canopy depth ranges between zero and LAI .

461 The three selected canopy depths are

462

$$l_i = \{0.5 - \sqrt{0.15}, \quad 0.5, \quad 0.5 + \sqrt{0.15}\} \cdot LAI, i = \{1, \quad 2, \quad 3\} \quad (7)$$

463

464 The gross leaf assimilation rate at a whole canopy level $A_{L,C}$ [$\text{kg}(\text{CO}_2) \text{m}^{-2}(\text{leaf}) \text{s}^{-1}$] is
465 described by

466

$$A_{L,C} = \frac{A_{L,l_1} + 1.6 \cdot A_{L,l_2} + A_{L,l_3}}{3.6} \quad (8)$$

467

468 where A_{L,l_1} , A_{L,l_2} and A_{L,l_3} [$\text{kg}(\text{CO}_2) \text{m}^{-2}(\text{leaf}) \text{s}^{-1}$] are the gross leaf assimilation rates of the
469 selected three leaf layers from up to down, respectively. The integrated value is obtained by
470 applying a weighting factor of 1.6 to the value at the canopy depth of $0.5 \cdot LAI$ and 1.0 to both
471 other values.

472

473 ***Leaf area expansion***

474

475 During the early stages of crop growth, leaf area expansion is mainly controlled by
 476 temperature through its effects on cell division and extension, rather than by the supply of
 477 assimilates. Leaf area increases more or less exponentially over time. In the later development
 478 stages, leaf area expansion is increasingly restricted by assimilate supply (Spitters et al., 1989).
 479 As reviewed by (Marcelis, Heuvelink, & Goudriaan, 1998), simulating leaf area on the basis of
 480 simulated leaf biomass increment and the SLA of new leaves has been used in several models.
 481 The crop growth in the early stages is essentially sink-limited, equivalent to growing in quite
 482 low temperatures and high radiation levels. This situation can also be described by the simulated
 483 leaf dry mass variation and the SLA of new leaves that imply the sink inhibition implemented
 484 by the buffer. Hence LAI [m^2 (leaf) m^{-2} (ground)] is uniformly described by

$$\frac{dLAI}{dt} = \frac{dX_d}{dt} \cdot (1 - \sigma_r) \cdot SLA \quad (9)$$

486

487 The SLA was defined as a function of irradiance, ambient temperature and CO_2
 488 concentration in TOMGRO models (Dayan et al., 1993a; Jones, Dayan, Allen, van Keulen, &
 489 Challa, 1991). Further, it depends mainly on temperature and is much less affected than by
 490 irradiance and CO_2 concentration (Dayan et al., 1993b). Gary, Barczi, Bertin, and Tchamitchian
 491 (1994) and Gijzen et al. (1997) proposed to use temperature and physiological age to describe
 492 the leaf expansion rate. However, according to the model calibration at the sub-model level in
 493 Section 2.2.5, radiation shows a much stronger correlation with SLA than temperature. In
 494 addition, when air is dry, cell elongation is reduced, leading to smaller leaves. Larger and
 495 thinner lettuce leaves are produced at high relative humidity (Bradbury & Ahmad, 1996;
 496 Tibbitts & Bottenberg, 1976). Hence, in this model, SLA [m^2 (leaf) kg^{-1} (leaf)] depends on
 497 radiation, humidity and a reference SLA .

498

$$SLA = SLA_{ref} \cdot f_{I,SLA} \cdot f_{Xh,SLA} \quad (10)$$

499

500 Referring to the expression form of climate determinant factor for SLA by Jones et al. (1991),

501 $f_{I,SLA}$ [-] is described by

502

$$f_{I,SLA} = \frac{1}{1 + \beta_I \cdot (I_{a,L,ref} - I_a/LAI)} \quad (11)$$

503

504 Similarly, $f_{Xh,SLA}$ [-] is described by

505

$$f_{Xh,SLA} = \frac{1}{1 + \beta_{Xh} \cdot (X_{h,ref} - X_h)} \quad (12)$$

506

507 ***Photosynthesis-light response***

508

509 The gross assimilation rate of individual leaves A_L [$\text{kg}(\text{CO}_2) \text{m}^{-2}(\text{leaf}) \text{s}^{-1}$] can be described

510 by a negative exponential photosynthesis-light response curve (Goudriaan & van Laar, 1994;

511 Spitters et al., 1989; van Ooteghem, 2010)

512

$$A_L = A_{L,sat} \cdot \left(1 - e^{-\frac{\varepsilon \cdot PAR_a}{A_{L,sat}}}\right) \quad (13)$$

513

514 On the basis of the photosynthesis-light response of individual leaves, the A_L in a specific

515 leaf layer located by canopy depth l_i , that is A_{L,l_i} , is calculated by substituting PAR_a for the

516 absorbed PAR by this specific leaf layer PAR_{a,l_i} . The PAR_{a,l_i} [$\text{W m}^{-2}(\text{leaf})$] is described by

517

$$PAR_{a,l_i} = k_{PAR} \cdot (1 - c_{r,PAR}) \cdot I \cdot \sigma_{PAR} \cdot e^{-k_{PAR} \cdot l_i} \quad (14)$$

518

519 To save computing time, the direct and diffuse radiations, as well as the sunlit and shaded
 520 leaves, are not distinguished. Their influences on crop photosynthesis are not involved in this
 521 model.

522

523 The effect of photorespiration on the light use efficiency ε [kg (CO₂) J⁻¹ (absorbed)] is
 524 described by (van Henten, 1994a)

525

$$\varepsilon = \varepsilon_0 \cdot \frac{X_c - \Gamma}{X_c + 2 \cdot \Gamma} \quad (15)$$

526

527 The CO₂ compensation point deals with photorespiration and dark respiration. For simplicity,
 528 dark respiration is assumed to be suppressed in the light. Then Γ is the CO₂ compensation
 529 concentration in the absence of dark respiration, which accounts for photorespiration at high
 530 light levels.

531

532 Higher temperatures strongly stimulate photorespiration by a faster increase in the affinity
 533 of rubisco to oxygen than to CO₂. The Γ [μ mol (CO₂) mol⁻¹ (air)] is affected by the canopy
 534 temperature T_c according to the following relation (Goudriaan & van Laar, 1994)

535

$$\Gamma = \Gamma_{T20} \cdot Q_{10,\Gamma}^{\frac{T_c - 20}{10}} \quad (16)$$

536

537 The gross leaf assimilation rate at light saturation $A_{L,sat}$ [$\text{kg}(\text{CO}_2) \text{m}^{-2}(\text{leaf}) \text{s}^{-1}$] is determined
 538 by adding the net leaf assimilation rate at light saturation $A_{L,sat,n}$ and the leaf maintenance
 539 respiration,

$$A_{L,sat} = A_{L,sat,n} + \frac{1}{c_\alpha} \cdot \frac{R_d}{LAI} \quad (17)$$

541
 542 The light saturated net assimilation rate $A_{L,sat,n}$ [$\text{kg}(\text{CO}_2) \text{m}^{-2}(\text{leaf}) \text{s}^{-1}$] is described by a
 543 simple Blackman-type approach (Farquhar, von Caemmerer, & Berry, 1980; Goudriaan & van
 544 Laar, 1994; van Ooteghem, 2010),

$$A_{L,sat,n} = \min(A_{L,c,n}, A_{L,mm}) \quad (18)$$

546

$$A_{L,c,n} = \frac{\rho_{CO_2} \cdot (X_c - \Gamma)}{r_{CO_2}} \cdot 10^{-6} \quad (19)$$

547

$$\rho_{CO_2} = \rho_{CO_2,0} \cdot \frac{T_{0,K}}{T_{c,K}} \quad (20)$$

548

$$A_{L,mm} = \frac{M_{CO_2} \cdot J_{max}}{4} \cdot 10^{-6} \quad (21)$$

549

$$J_{max} = J_{max,25} \cdot e^{E_J \cdot \frac{T_{c,K} - T_{25,K}}{T_{c,K} \cdot R_g \cdot T_{25,K}}} \cdot \frac{1 + e^{\frac{c_S \cdot T_{25,K} - c_H}{R_g \cdot T_{25,K}}}}{1 + e^{\frac{c_S \cdot T_{c,K} - c_H}{R_g \cdot T_{c,K}}}} \quad (22)$$

550

551 ***Leaf resistance***

552

553 The total leaf resistance for CO₂ transport from ambient air to the chloroplast is determined
 554 by adding stomatal, boundary layer and carboxylation resistances. When the CO₂ concentration
 555 is measured above the canopy, the so-called turbulence resistance must be added because the
 556 CO₂ concentration in free air is less variable than that within the canopy (Goudriaan, 1982; Yin
 557 & van Laar, 2005). Cuticular resistance, parallel to the stomatal resistance (Bot, 1983), also
 558 exists. However, it is much larger than stomatal resistance (Monteith & Unsworth, 2013). The
 559 contribution of the cuticle resistance to CO₂ transfer is ignored in this research. Then, the total
 560 leaf resistance to CO₂ diffusion r_{CO_2} [s m⁻¹] is described by

$$r_{CO_2} = r_s + r_b + r_c + r_t \quad (23)$$

562
 563 In the literature, the stomatal and boundary layer resistances are often assumed constant for
 564 photosynthesis rate simulation. However, van Ooteghem (2010) found that the photosynthesis
 565 models with dynamic resistances give a better description than those with constant resistances.
 566 During photosynthesis, CO₂ molecules follow the same path as water vapour (H₂O) but in the
 567 opposite direction. The dynamic resistances to CO₂ diffusion are mainly determined with an
 568 evaporation model that holds equations for the stomatal and boundary layer resistances to H₂O
 569 by Stangheilini (1987). Then, the stomatal resistance to CO₂ diffusion r_s [s m⁻¹] is described by

$$r_s = c_\zeta \cdot r_{H_2O,min} \cdot f_{l,s} \cdot f_{Tc,s} \cdot f_{Xc,s} \cdot f_{Xh,s} \quad (24)$$

571
 572 The radiation, temperature, CO₂, and humidity dependencies for stomatal resistance are
 573 described by

574

$$f_{I,s} = \frac{\frac{I_a}{2 \cdot LAI} + 4.30}{\frac{I_a}{2 \cdot LAI} + 0.54} \quad (25)$$

575

$$f_{Tc,s} = \begin{cases} 1 + 0.5 \cdot 10^{-2} \cdot (T_c - 33.6)^2, & I \leq 3 \\ 1 + 2.3 \cdot 10^{-2} \cdot (T_c - 24.5)^2, & I > 3 \end{cases} \quad (26)$$

576

$$f_{Xc,s} = \begin{cases} 1, & I \leq 3 \\ 1 + 6.1 \cdot 10^{-7} \cdot (X_c - 200)^2, & I > 3 \wedge X_c < 1100 \\ 1.5, & I > 3 \wedge X_c \geq 1100 \end{cases} \quad (27)$$

577

$$f_{Xh,s} = \frac{4}{(1 + 255 \cdot e^{-0.54 \cdot 10^{-2} \cdot e_{c,a}})^{0.25}} \quad (28)$$

578

579 Differing from absorbed PAR per leaf area for a specific leaf layer in the canopy, I_a [W m^{-2}
580 (ground)], which represents absorbed shortwave radiation by canopy, is calculated by

581

$$I_a = (1 - c_{r,I}) \cdot I \cdot (1 - e^{-k_I \cdot LAI}) \quad (29)$$

582

583 Since canopy temperature is assumed to be equal to air temperature and vapour pressure in
584 leaves is always saturated, $e_{c,a}$ is equal to vapour pressure deficit (VPD) of greenhouse air. Then
585 the leaf to air vapour pressure difference $e_{c,a}$ [Pa] could be described by

586

$$e_{c,a} = e_{s,air} \cdot (1 - X_h) \quad (30)$$

587

588 And the saturated vapour pressure of greenhouse air $e_{s,air}$ [Pa] is described by (Stanghellini
589 et al., 2019)

590

$$e_{s,air} = \begin{cases} 10^{2.7857 + \frac{9.5 \cdot X_t}{265.5 + X_t}}, & X_t < 0 \\ 10^{2.7857 + \frac{7.5 \cdot X_t}{237.3 + X_t}}, & X_t \geq 0 \end{cases} \quad (31)$$

591

592 The resistance offered by the boundary layer depends on leaf dimensions and windspeed.
 593 The boundary layer resistance to CO₂ diffusion r_b [s m⁻¹], which is derived from that to
 594 convective heat transfer, is described by

595

$$r_b = Le^{0.67} \cdot \frac{1174 \cdot l_f^{0.5}}{(l_f \cdot |T_c - X_t| + 207 \cdot v_a^2)^{0.25}} \quad (32)$$

596

597 where Le [-] is the Lewis number for CO₂ in air at 25 °C. $Le^{0.67}$ represents the ratio of
 598 boundary layer resistance for CO₂ diffusion to that for forced heat convection. l_f [m] is the leaf
 599 characteristic dimension, taken as the mean leaf width in the wind direction (Schuepp, 1993).

600

601 van Henten (1994a) used a second-order polynomial fitting to describe the carboxylation
 602 resistance. This polynomial only works within an air temperature range from 5 to 40 °C. The
 603 description of carboxylation resistance by Goudriaan and van Laar (1994) and van Ooteghem
 604 (2010) covers a wider temperature range. It is also more explanatory, since it defines the
 605 carboxylation resistance as the ratio of the effective Michaelis Menten constant for
 606 carboxylation to the maximum carboxylation rate, both of which are derived from Farquhar et
 607 al. (1980). In this model, we use a descriptive function of temperature like that by van Henten
 608 (1994a) but derived from the simulation result by van Ooteghem (2010) to describe the leaf
 609 carboxylation resistance r_c [s m⁻¹],

610

$$r_c = c_{rc,1} \cdot T_c^2 + c_{rc,2} \cdot T_c + c_{rc,3} \quad (33)$$

611

612 ***Respiration***

613

614 Some carbohydrates formed are respired to provide energy for maintaining the existing
615 biostructures. The crop maintenance respiration rate R_d [kg (CH₂O) m⁻² (ground) s⁻¹] is
616 described by

617

$$R_d = R_{d,25} \cdot Q_{10,Rd}^{\frac{T_c-25}{10}} \quad (34)$$

618

619 Based on the typical values for the maintenance coefficients of various plant organs used by
620 van Keulen, Penning de Vries, and Drees (1982), $R_{d,25}$ [kg (CH₂O) m⁻² (ground) s⁻¹] is described
621 by

622

$$R_{d,25} = (c_{Rd,25,sh} \cdot (1 - \sigma_r) + c_{Rd,25,r} \cdot \sigma_r) \cdot X_d \quad (35)$$

623

624 ***Shoot/ root ratio***

625

626 The ratio of shoot to root dry weight depends on cumulative dry matter partitioning during
627 growth, primarily regulated by the sink strengths of plant organs. The sink strength is quantified
628 by the maximum growth rate of the organ (Marcelis, 1996), which mainly depends on the
629 development stage or heat sum (Penning De Vries & van Laar, 1982). Development stages are
630 usually distinguished based on major phenological events, such as emergence (0), anthesis (1)
631 and ripening (2) (Goudriaan & van Laar, 1994). In greenhouse lettuce cultivation, growth
632 simulation focuses on the development stage between 0 and 1, starting from transplanting.
633 Hence, Lazof, Bernstein, and Lauchli (1991) used the leaf plastochron index to define this stage.

634 As reviewed by Bakker, Bot, Challa, and van de Braak (1995), dry matter distribution towards
635 roots generally decreases with plant size. Instead of calculating leaf and root dry weights by
636 integration based on the partitioning factors that depend on the development stage, the root ratio
637 σ_r [-] described as a function of the individual plant dry weight, is adopted. It is largely
638 simplified and assumed to be accurate enough to determine the shoot/ root ratio for the leafy
639 vegetable.

640

$$\sigma_r = c_{\sigma r,1} \cdot \ln\left(\frac{X_d}{\rho_c}\right) + c_{\sigma r,2} \quad (36)$$

641

642 **2.2.3. Source code**

643 The code used for the design, simulation, and visualisation of the lettuce growth model is
644 available in MATLAB format (MATLAB R2021b, The MathWorks) at Mendeley Data
645 (<http://dx.doi.org/10.17632/r7z9ttvkyh.2>). The inputs of this code template, including
646 greenhouse climates, initial crop states, and plant density, are from Exp_v2. This open source
647 code allows readers to understand, use, and improve our model conveniently.

648

649 **2.2.4. Model evaluation method**

650

651 The differential equations were solved with the ODE45 solver in MATLAB software to
652 simulate crop growth. Greenhouse climate data with 5-minute intervals were used as model
653 inputs. Model performances were evaluated by comparing the measured and simulated crop dry
654 weights, using the root mean square error (RMSE) and relative root mean square error
655 (RRMSE). The two common metrics are defined as follows,

656

$$RMSE = \sqrt{\frac{1}{n} \sum_{i=1}^n (y_i^m - y_i^s)^2} \quad (37)$$

657

$$RRMSE = \frac{100}{\overline{y^m}} \sqrt{\frac{1}{n} \sum_{i=1}^n (y_i^m - y_i^s)^2} \quad (38)$$

658

659 where y_i^m and y_i^s are measured and simulated values at the same timepoint, n is the number of
 660 measurements, $\overline{y^m}$ is the average of measured values. While the RMSE measures the absolute
 661 magnitude of prediction errors, the RRMSE expresses the error as a percentage relative to the
 662 sample mean. The latter allows us to deal with datasets with different units or scales and
 663 compare the performance across crop models. Taking reference from the evaluation of a field
 664 crop model (Jamieson, Porter, & Wilson, 1991), the performance of modelling lettuce growth
 665 is considered to be excellent if RRMSE < 10%, good if the RRMSE is between 10% and 20%,
 666 acceptable if the RRMSE is between 20% and 30%, and poor if RRMSE > 30%.

667

668 Following the criteria for publishing crop model papers (Sinclair & Seligman, 2000), the
 669 prediction of the critical crop growth indicator, leaf area index (LAI), throughout the simulated
 670 growth cycle was also considered in the model evaluation. Additionally, the simulation and
 671 presentation of another state variable, the amount of stored carbohydrates in the buffer, were
 672 conducted to assess the role of the model framework and underlying hypothesis.

673

674 **2.2.5. Parameter estimation and calibration**

675 All the parameters of the lettuce growth model, including their values and sources, are listed
 676 in Table 2. These parameters remained constant throughout the simulations and are expected to
 677 apply to future model applications in greenhouse management for lettuce cultivation. Most of

678 them were derived directly or estimated from the literature. Some model parameters were
679 determined by means of model calibration at both the sub-model and model levels. The others
680 were determined from physical properties. The choice of some of the parameters is motivated
681 as follows.

682

683 Table 2 Parameterisation of the lettuce crop growth model

Parameter	value	unit	source
C_H	2.2×10^5	J mol^{-1}	Farquhar et al. (1980)
$C_{r,1}$	0.22	-	Goudriaan and van Laar (1994)
$C_{r,PAR}$	0.07	-	Marcelis et al. (1998)
$C_{rc,1}$	0.315	$\text{m s}^{-1} \text{ } ^\circ\text{C}^{-2}$	estimated from van Ooteghem (2010)
$C_{rc,2}$	-27.35	$\text{m s}^{-1} \text{ } ^\circ\text{C}^{-1}$	estimated from van Ooteghem (2010)
$C_{rc,3}$	790.7	m s^{-1}	estimated from van Ooteghem (2010)
$C_{Rd,25,r}$	1.16×10^{-7}	$\text{kg (CH}_2\text{O) kg (dry matter) s}^{-1}$	van Keulen et al. (1982)
$C_{Rd,25,sh}$	3.47×10^{-7}	$\text{kg (CH}_2\text{O) kg (dry matter) s}^{-1}$	van Keulen et al. (1982)
C_S	710	$\text{J mol}^{-1} \text{ K}^{-1}$	Farquhar et al. (1980)
C_α	0.68	-	physical constant
C_β	0.8	-	van Henten (1994a)
C_ζ	1.6	-	Goudriaan (1982)
$C_{\sigma,1}$	-0.026	plants kg^{-1}	sub-model calibration
$C_{\sigma,2}$	-0.076	-	sub-model calibration
E_J	3.7×10^4	J mol^{-1}	van Ooteghem (2010)
$I_{a,L,ref}$	50.3	W m^{-2} (leaf)	sub-model calibration
$J_{max,25}$	210.15	$\mu\text{mol (e}^-) \text{ m}^{-2}$ (leaf) s^{-1}	van Ooteghem (2010)
k_I	0.48	-	van Ooteghem (2010)
k_{PAR}	0.9	-	van Henten (1994a)

Le	1.47	-	Monteith and Unsworth (2013)
l_f	0.1	m	measurement
M_{CO_2}	44×10^{-3}	kg mol ⁻¹	physical constant
$Q_{10,gr}$	1.6	-	Sweeney et al. (1981)
$Q_{10,Rd}$	2	-	Goudriaan and van Laar (1994)
$Q_{10,\Gamma}$	2	-	Goudriaan and van Laar (1994)
R_g	8.314	J mol ⁻¹ K ⁻¹	physical constant
$RGR_{max,20}$	1.54×10^{-6}	s ⁻¹	global calibration
$r_{H_2O,min}$	82	s m ⁻¹	Stanghellini (1987)
r_t	50	s m ⁻¹	Goudriaan (1982)
SLA_f	47.93	m ² (leaf) kg ⁻¹ (leaf)	sub-model calibration
$T_{c,RGR}$	25	°C	global calibration
v_a	0.09	m s ⁻¹	van Ooteghem (2010)
$X_{h,ref}$	0.75	-	sub-model calibration
β_l	-4.74×10^{-3}	m ² (leaf) W ⁻¹	sub-model calibration
β_{Xh}	0.912	-	sub-model calibration
ϵ_0	17×10^{-9}	kg (CO ₂) J ⁻¹	Goudriaan et al. (1985)
$\rho_{CO_2,T0}$	1.98	kg m ⁻³	physical constant
σ_{buf}	0.2	-	estimated from Goudriaan et al. (1985)
σ_{PAR}	0.5	-	Stanghellini et al. (2019)
Γ_{T20}	40	μmol (CO ₂) mol ⁻¹ (air)	Goudriaan and van Laar (1994)

684

685 According to Goudriaan et al. (1985), if the plant lacks adequate sinks, an increase in buffer
686 storage exceeding 20% on a dry matter basis will reduce the assimilation rate. Thus, the ratio
687 of the maximum buffer capacity to crop dry weight σ_{buf} was set to 0.2. In addition, the primary
688 assimilates in excess of the maintenance costs are converted into structural plant material.
689 Considering the little difference in assimilate requirements to form a unit weight of leaves and
690 roots (Spitters et al., 1989), the conversion factor of a lettuce crop $c_\beta = 0.8$ was set at the whole

691 plant level (van Henten, 1994a). Hence, the crop growth simulation can take the dry matter as
692 substrates of the partition process rather than the primary carbohydrates by photosynthesis,
693 which is the actual situation.

694 The response of leaf carboxylation resistance r_c to canopy temperature T_c was described by
695 quadratic polynomial fitting in the range of 0 to 50 °C (Fig. 4). The temperature interval for
696 fitting was 0.1 °C, and the corresponding carboxylation resistance data were derived from the
697 simulation result of the model by van Ooteghem (2010). Coefficients of the quadratic term $c_{rc,1}$,
698 linear term $c_{rc,2}$, and constant term $c_{rc,3}$ were estimated to be $0.315 \text{ m s}^{-1} \text{ °C}^{-2}$, $-27.35 \text{ m s}^{-1} \text{ °C}^{-1}$,
699 and 790.7 m s^{-1} .

700 X_d / ρ_c [kg per plant] represents the individual plant dry weight. With its increase, the root
701 ratio decreases logarithmically (Fig. 5). To make the model parameters more universal, data
702 from three experiments were used to estimate the coefficients of the logarithmic function. The
703 coefficients of $c_{or,1}$ and $c_{or,2}$ were calculated to be $-0.026 \text{ m}^2 \text{ kg}^{-1}$ and -0.076 , respectively.

704 It is not easy to measure biomass and leaf area as frequently as measuring greenhouse climate
705 (e.g., sampling every 5 minutes). The available crop data for calibrating the sub-model that
706 describes the SLA of new leaves were sampled every five days. Thus, the SLA and LAI data
707 were taken from the difference and average of two adjacent samples, respectively. Accordingly,
708 the climate data used for calibration were averaged over five days, and only daytime data were
709 counted since new leaves are mainly generated under the light. Calibration using average
710 climate data is accepted since, as defined by Eq. (11) and (12), the effects of absorbed shortwave
711 radiation per leaf area and air humidity on SLA are respectively assumed to be linear. First,
712 linear fitting slopes were calculated as $-0.227 \text{ m}^4 \text{ kg}^{-1} \text{ W}^{-1}$ for radiation and $43.69 \text{ m}^2 \text{ kg}^{-1}$ for
713 humidity. Compared with temperature ($R^2 = 0.122$, RMSE = 11.569), radiation ($R^2 = 0.351$,
714 RMSE = 9.947) and humidity ($R^2 = 0.247$, RMSE = 10.712) showed stronger correlations with
715 SLA . Second, β_I and β_{Xh} were expressed by $-0.227/SLA_{ref} [\text{m}^2 \text{ W}^{-1}]$ and $43.69/SLA_{ref} [-]$ for

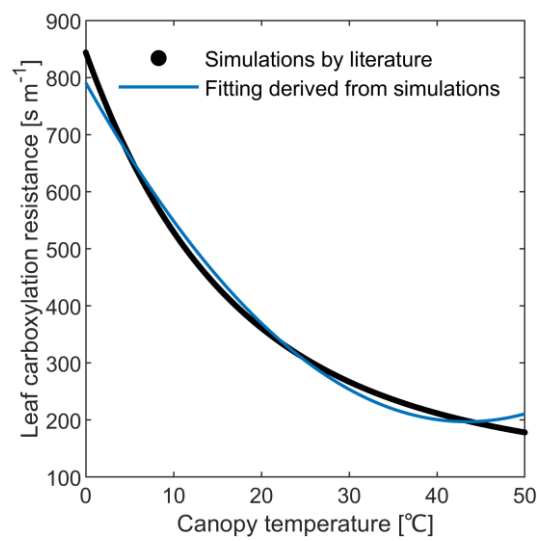
716 calibration since they make sense only for a specific reference SLA . Third, SLA_{ref} , $I_{a,L,ref}$, $X_{h,ref}$
717 were estimated to be 47.93 m² (leaf) kg⁻¹ (leaf), 50.3 W m⁻² (leaf), and 0.75 by fitting (Fig. 6)
718 in the functional form of Eq. (10)-(12). Also, β_I and β_{Xh} were determined as -4.74×10^{-3} m² W⁻¹
719 and 0.912.

720 Two parameters, the maximum relative growth rate of dry matter at 20 °C ($RGR_{max,20}$), and
721 the temperature to achieve the saturation relative growth rate ($T_{c,RGR}$), were determined by
722 global calibration. The global calibration, using data from Exp_c, aimed to minimise the
723 RRMSE between the measured and simulated crop dry weights. A grid search method was used
724 for reference to limit the range of parameters and traverse the parameter combinations.
725 $RGR_{max,20}$ and $T_{c,RGR}$ were calibrated to be 1.54×10^{-6} s⁻¹ and 25 °C, achieving the minimum
726 RRMSE of 16.8%.

727 Fig. 7 presents greenhouse climate inputs and the simulation result based on Exp_c
728 conducted during the cold season. Although growers made great efforts to regulate the
729 greenhouse climate for lettuce cultivation, extreme thermal environments frequently occur,
730 which is common in current standard CSGs. The simulation spanned 50 consecutive days, with
731 the average air temperature of 18.2 °C during the day and 7.9 °C at night. The extremely low
732 temperatures below 5 °C constituted 16% of the period and even briefly dropped to below zero
733 in two nights with a minimum of -1.0 °C. Low temperatures were the main temperature stress
734 in this calibration experiment. Over the simulation, the average humidity was 58% and 93% in
735 the daytime and nighttime. Extremely high humidity levels, indicated by VPD lower than 0.2
736 kPa (Stanghellini et al., 2019), accounted for 65% of the period, whereas extremely low
737 humidity, with VPD higher than 1.0 kPa, accounted for 16%. Humidity stress, especially high
738 humidity stress, occupied most of this period. Daily cumulative radiation was measured to be
739 1.9-6.9 MJ m⁻² d⁻¹, with an average of 5.6 MJ m⁻² d⁻¹. CO₂ was supplemented by natural
740 ventilation, maintaining an average concentration of 533 μmol mol⁻¹ during the day and 614

741 $\mu\text{mol mol}^{-1}$ at night. In the early stages of lettuce growth, the daytime CO_2 concentration
742 exceeding $400 \mu\text{mol mol}^{-1}$ might be due to the decomposition of organic bottom fertiliser. The
743 simulated dry matter weights closely mirrored the measured values, and underestimation
744 existed except for the harvest timepoint. Through model calibrations at both sub-model and
745 model levels, the model performance was evaluated to be good in simulating lettuce dry weight,
746 with $\text{RRMSE} = 16.8\%$ and $\text{RMSE} = 0.0081 \text{ kg m}^{-2}$ (ground).

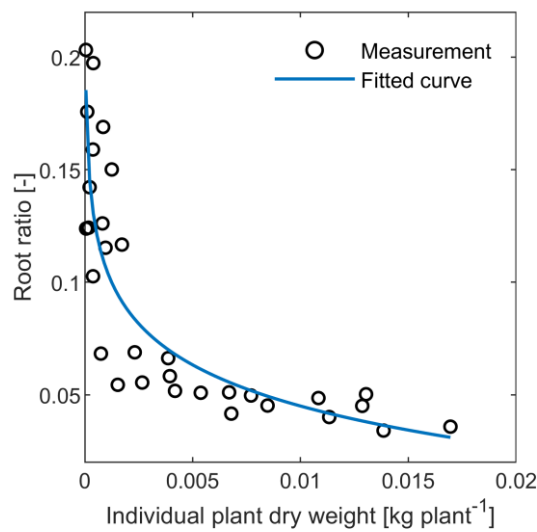
747



748

749 Fig. 4 Fitting of the leaf carboxylation resistance. $R^2 = 0.992$, $\text{RMSE} = 15.996$.

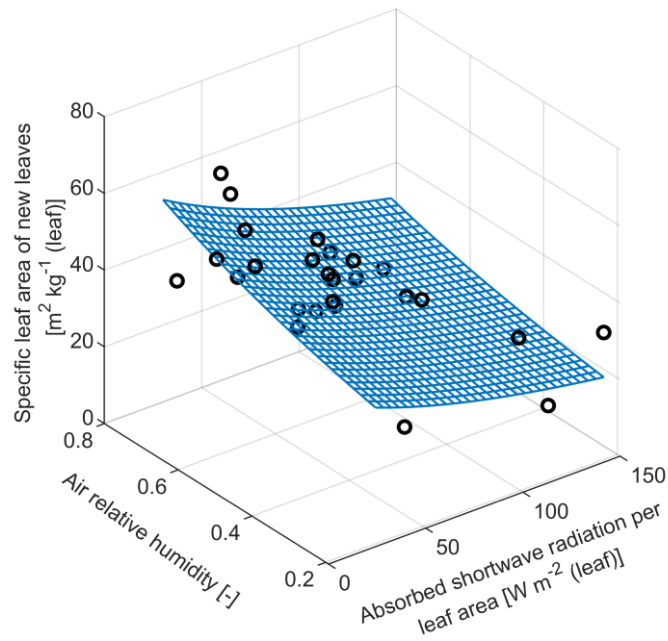
750



751

752 Fig. 5 Root ratio variation along with the individual plant dry weight. $R^2 = 0.726$, RMSE =
753 0.028.

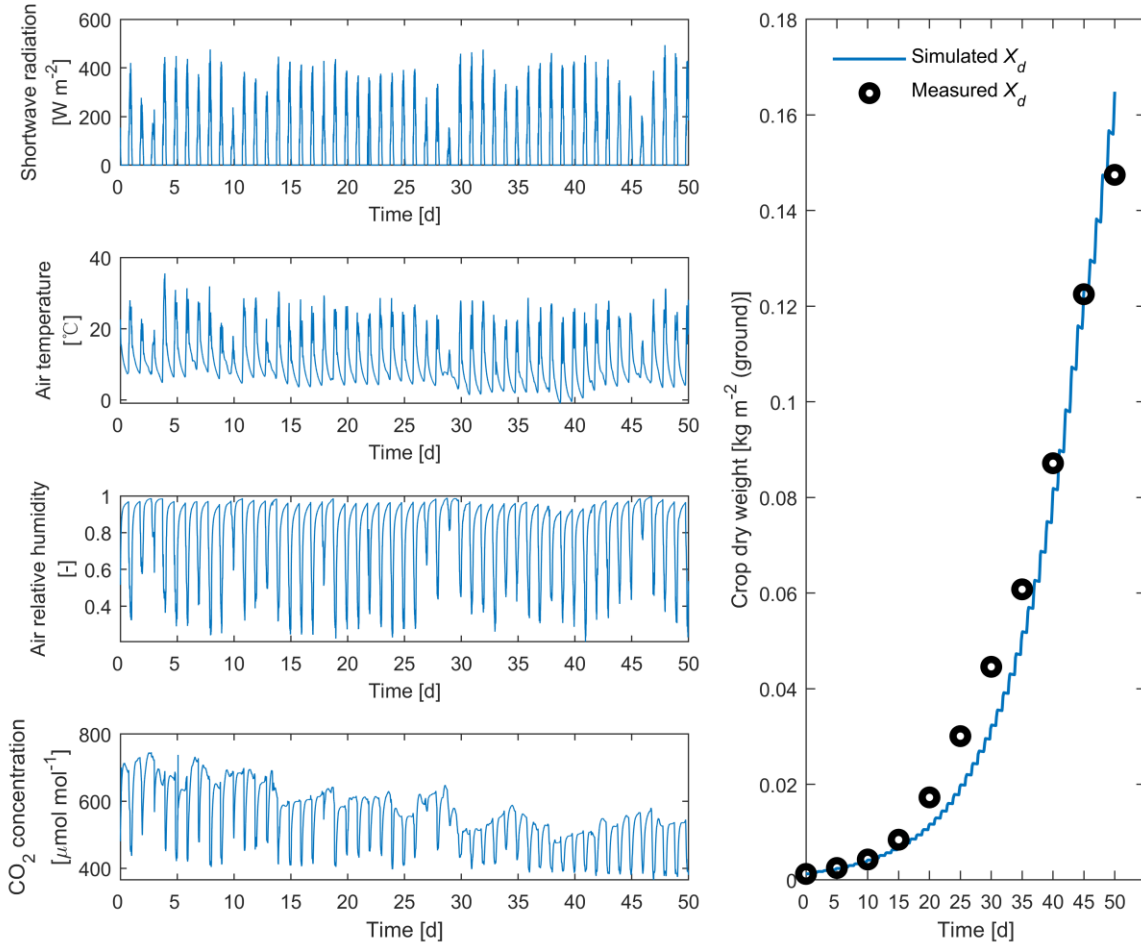
754



755

756 Fig. 6 Effects of absorbed shortwave radiation by leaves and air humidity on the specific leaf
757 area of new leaves. $R^2 = 0.380$, RMSE = 9.928.

758



759

760

761

762

763

764

3. Results

765

3.1. Model validation

766

767

768

769

770

The model was validated using the observed data from Exp_v1 and Exp_v2. The model parameters in the validation simulations were kept constant with those (Table 2) contributed by the global calibration using data from Exp_c. The model inputs included the greenhouse climate (I , X_c , X_t , and X_h), initial crop states (X_d , LAI , and C_{buf}), and plant density ρ_c . The initial X_d and LAI were measured values, while the initial C_{buf} was set to be 0 kg m^{-2} (Table 1). The model

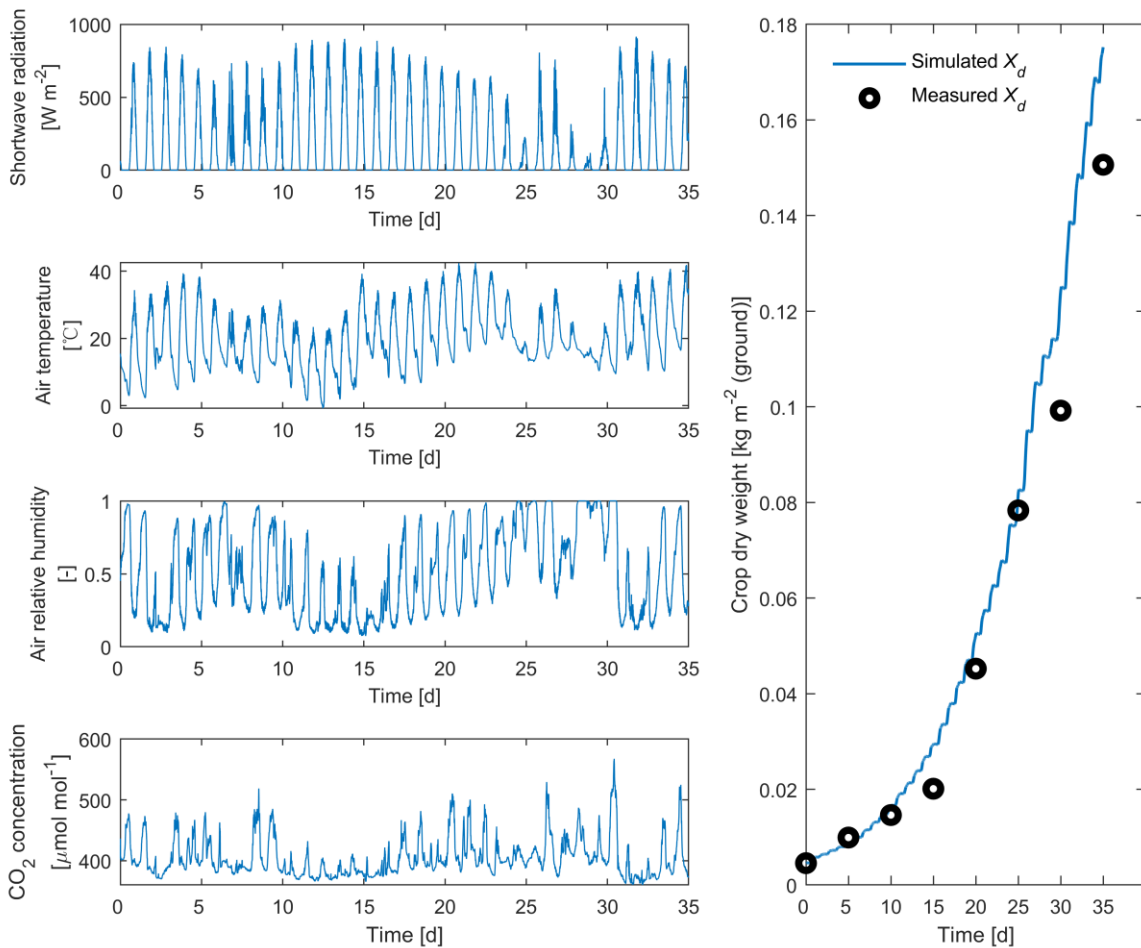
771 validation mainly compared the measured and simulated values of the crop dry weight,
772 representing the state of lettuce growth in this study.

773 Fig. 8 presents greenhouse climate inputs and the model validation result based on Exp_v1
774 conducted during the warm season. The simulation spanned 35 consecutive days, from lettuce
775 transplanting to harvesting, with the average air temperature of 24.3 °C during the day and 14.1 °C
776 at night. The temperatures exceeding 30 °C constituted 17% of the period, reaching a maximum
777 of 42.6 °C, while the extremely low temperatures below 5 °C constituted only 3%, with a
778 minimum of -0.8 °C. High temperatures were the primary temperature stress during Exp_v1.
779 Over this validation process, the average humidity was 41% and 65% in the daytime and
780 nighttime. Extremely high humidity levels, indicated by VPD lower than 0.2 kPa, accounted
781 for 19% of the period, whereas extremely low humidity, with VPD higher than 1.0 kPa,
782 accounted for 51%. Humidity stress, especially the low humidity stress, dominated this period.
783 Daily cumulative radiation was measured to be 1.7-21.3 MJ m⁻² d⁻¹, with an average of 15.5 MJ
784 m⁻² d⁻¹. CO₂ was supplemented by natural ventilation, maintaining an average concentration of
785 396 μmol mol⁻¹ during the day and 417 μmol mol⁻¹ at night. The simulated dry matter weights
786 closely agreed with the measured values, with an overall overestimation. The model
787 performance was acceptable in simulating the crop dry weight of the lettuce, with RRMSE =
788 24.9% and RMSE = 0.0131 kg m⁻² (ground).

789 Fig. 9 presents greenhouse climate inputs and the model validation result based on Exp_v2
790 conducted during the cold-warm season. The simulation spanned 45 consecutive days, with the
791 average air temperature of 20.9 °C during the day and 11.7 °C at night. The temperatures
792 exceeding 30 °C constituted 4% of the period, reaching a maximum of 36.0 °C, while the
793 extremely low temperatures below 5 °C constituted only 1%, with a minimum of 3.9 °C. The
794 greenhouse climate was generally mild in Exp_v2. Over this validation process, the average
795 humidity was 60% and 95% in the daytime and nighttime. Extremely high humidity levels

796 accounted for 61% of the period, whereas extremely low humidity accounted for 21%.
 797 Humidity stress, especially the high humidity stress, occupied most of this period. Daily
 798 cumulative radiation was measured to be 0.8-13.3 MJ m⁻² d⁻¹, with an average of 8.8 MJ m⁻² d⁻¹.
 799 CO₂ maintained an average concentration of 395 μmol mol⁻¹ during the day and 490 μmol
 800 mol⁻¹ at night. The simulated dry matter weights closely mirrored the measured values with an
 801 overall underestimation. The model performance was good in simulating the crop dry weight
 802 of the lettuce, with RRMSE =10.5% and RMSE = 0.0070 kg m⁻² (ground).

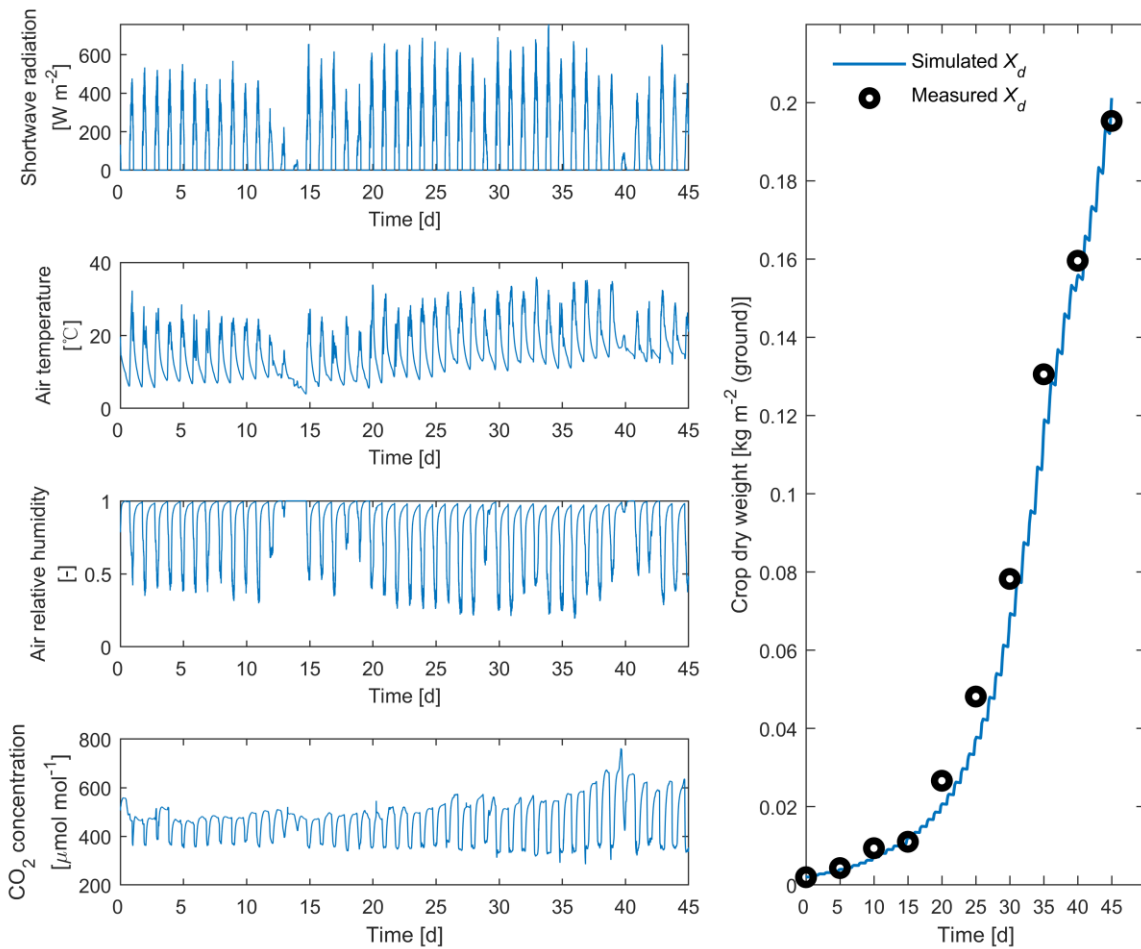
803



804

805 Fig. 8 Five minutes averages of the greenhouse climate measurements, as well as the
 806 measured and simulated crop dry weights during the first validation experiment. The simulation
 807 for model validation is from 17:00, 9 April 2020, to 17:00, 14 May 2020.

808



809

810 Fig. 9 Five minutes averages of the greenhouse climate measurements, as well as the
 811 measured and simulated crop dry weights during the second validation experiment. The
 812 simulation for model validation is from 15:00, 30 January 2022, to 15:00, 16 March 2022.

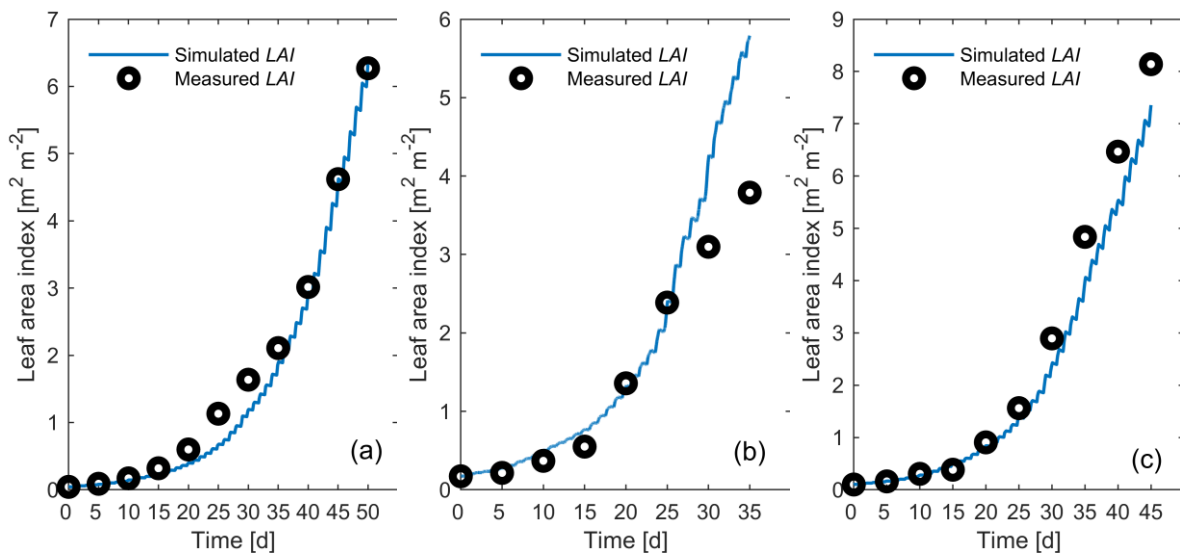
813

814 3.2. Leaf area index simulations

815 In this model, LAI is one of the state variables, and it affects dry matter accumulation by
 816 influencing the canopy photosynthesis rate. Additionally, LAI itself holds significant
 817 importance in greenhouse climate control as a preferred indicator for providing crop
 818 information feedback, since it spans the entire lettuce growth cycle and is easier to identify than
 819 biomass (Rahimikhoob, Delshad, & Habibi, 2023). In Exp_c (Fig. 10a), the simulated LAI
 820 values exhibited the same trend as the measurements, consistently underestimating until harvest
 821 time, where a slight overestimation occur. The model performance was good in simulating LAI,

822 with an RRMSE of 12.1% and an RMSE of $0.2196 \text{ m}^2 \text{ (leaf) m}^{-2} \text{ (ground)}$. In Exp_v1 (Fig.
 823 10b), the simulated LAI followed a similar trend to the measured values but showed great
 824 overestimations near harvest, resulting in an RRMSE of 54.7% and an RMSE of 0.8164. In
 825 Exp_v2 (Fig. 10c), the simulated LAI followed the same trend as the measured values, with an
 826 overall underestimation. The RRMSE was 19.5%, and the RMSE was 0.5019, indicating a good
 827 model performance in simulating LAI.

828



829

830 Fig. 10. LAI simulations of the lettuce growth model using data from the calibration
 831 experiment (a), the first validation experiment (b), and the second validation experiment (c).

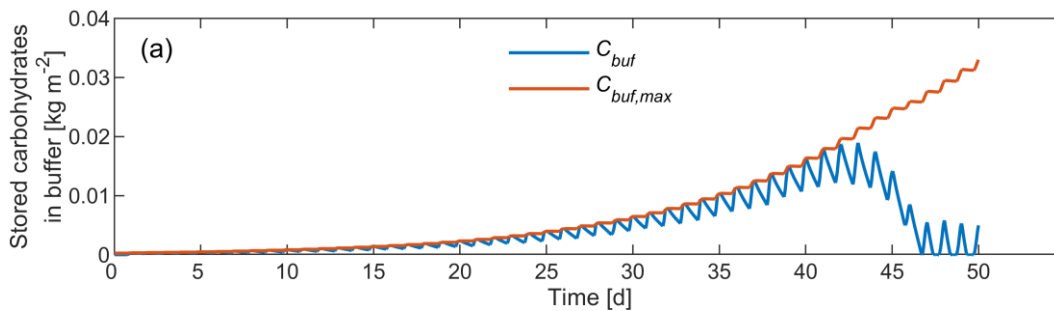
832

833 3.3. Buffer storage simulations

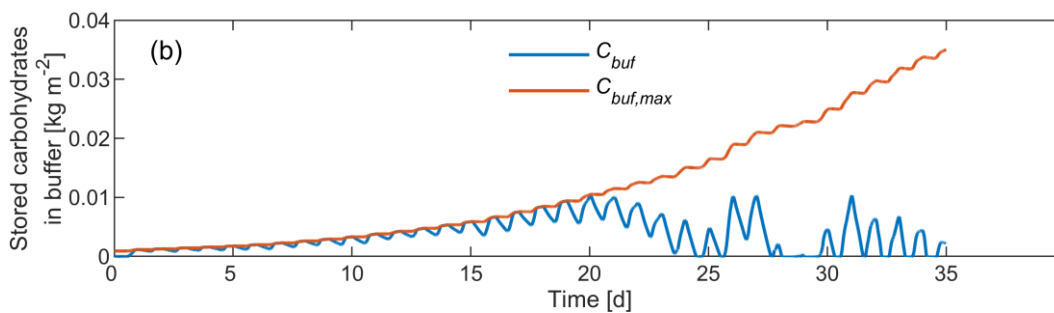
834 To fully describe the effects of adverse temperature conditions throughout the day, including
 835 extremely high and low temperatures, on crop growth, this study introduces a novel model
 836 framework that incorporates double parallel mass flows, along with the underlying hypothesis
 837 of buffer flows and canopy photosynthesis inhibition. Fig. 11 illustrates changes in
 838 carbohydrate storage within the buffer. As buffer storage reaches or surpasses its maximum
 839 capacity, photosynthesis inhibition will happen until it falls below the capacity. During this

840 state, the inhibition also becomes ineffective if the assimilation rate is lower than the combined
841 respiration and potential growth rates. The model programming allows the buffer storage to
842 exceed its maximum capacity at some point and then remain constant until the storage goes
843 below the capacity as a result of dry matter increase, effectively practising the model description.
844 In Exp_c, where the low temperature was the primary stress, photosynthesis inhibition lasted
845 until the 42nd day in the simulation, constituting 41% of the total photosynthesis duration. In
846 Exp_v1, with high temperature as the primary stress, inhibition lasted until the 20th day,
847 representing 27% of the total photosynthesis duration. In Exp_v2, with temperatures
848 transitioning from cold to warm, inhibition lasted until the 32nd day, representing 33% of the
849 total photosynthesis duration. Such inhibitions occur during vigorous photosynthesis in the
850 daytime.

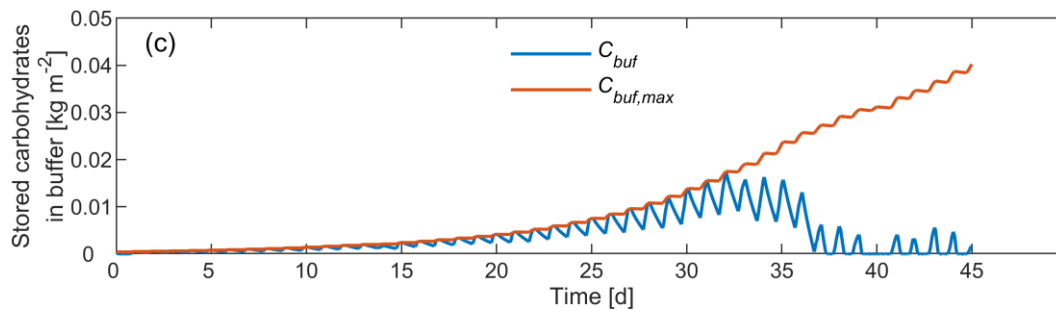
851



852



853



854

855 Fig. 11 Buffer storage variations based on data from the calibration experiment (a), the first
 856 validation experiment (b), and the second validation experiment (c).

857

858 4. Discussion

859 4.1. Insights from model evaluation

860 Through the three lettuce cultivation experiments in different seasons and greenhouses,
 861 specifically including an experiment for global calibration and two for validation, the model
 862 performance was evaluated (Fig. 7, Fig. 8, and Fig. 9). The greenhouse climate upon which the
 863 model evaluations were based was in a broad range, embodied in the complete coverage of
 864 temperature and humidity levels and climate varieties (0-915.6 W m⁻² for shortwave radiation,
 865 -1.0-42.6°C for air temperature, 7%-100% for relative humidity, and 285-762 μmol mol⁻¹ for
 866 CO₂ concentration). The evaluation results showed that the model performance was good and
 867 acceptable. In essence, the developed model can precisely depict the response of lettuce growth
 868 to the broad range of greenhouse climates, providing a foundational crop model for optimally
 869 managing greenhouse climate in lettuce production.

870 To the best of our knowledge, optimal control theory is not only applicable to modern multi-
 871 span greenhouses (van Straten et al., 2010) but also holds great potential for use in low-tech
 872 greenhouses, including those lacking climate conditioning devices or even operated manually.
 873 In such low-tech greenhouses, like CSGs and Mediterranean greenhouses (Vanthoor,
 874 Stanghellini, van Henten, & De Visser, 2011), the indoor climate is only partially controllable.
 875 They frequently experience extreme temperatures, and humidity levels cannot always be

876 maintained within ranges considered non-limiting to crop growth. Implementing optimal
877 control in these greenhouses, whether through online control or providing decision advice,
878 requires the crop model component to accurately simulate crop dynamics under extreme
879 thermal environments. As previously reviewed, existing mechanistic lettuce models are
880 inadequate for addressing this challenge (Critten, 1991; Pearson et al., 1997; van Henten,
881 1994a). The lettuce growth model of this study, with an innovative framework and extended
882 descriptions to address a broad range of greenhouse climates, enables optimal control for
883 various greenhouse types, including low-tech greenhouses with poor performance on climate
884 conditioning, and brings additional humidity effects into problem-solving. Meanwhile, it allows
885 optimal control to proactively explore extreme climate conditions, thereby expanding the range
886 of feasible solutions.

887 However, we cannot compare the developed model to others since none of the existing
888 lettuce growth models have reported the RRMSE for states. For instance, van Henten (1994a)
889 adopted assessment criteria stating that the simulated dry weight should fall within a 95%
890 confidence interval of the measured values for most of the time. Instead, almost all crop models
891 compared the dynamic trends between simulated and observed values, lacking a quantitative
892 index basis. This situation exists in other mainstream greenhouse crop models, such as tomato
893 yield modelling (Dayan et al., 1993b; Vanthoor, De Visser, Stanghellini, & van Henten, 2011).
894 Compared with greenhouse climate dynamics (Katzin, van Henten, & van Mourik, 2022), crop
895 growth processes are more complex and have more challenges in accurate predictions.
896 Meanwhile, it is difficult for crop models to obtain data for calibration and validation in seconds
897 or minutes. The quality of destructive samplings in a limited number, especially those
898 performed near the harvest time where larger deviations can occur, strongly impacts the
899 RRMSE calculation and model evaluation results. For example, in Exp_v1, the RRMSE for
900 crop dry weight could reach 17.5% if the last two samples were excluded. These may explain

901 the rare presentation of RRMSE values in current greenhouse crop models. This study provides
902 RRMSE values for simulating lettuce dry weight, which will benefit future comparative studies,
903 while a qualitative description of its dynamic trends throughout the growth period remains
904 essential.

905 Furthermore, in the global calibration aimed at minimising the RRMSE for crop dry weight,
906 adjustments to model parameters tended to restrain crop growth in the early stages to prevent
907 excessive growth during harvest. Consequently, the model consistently underestimated dry
908 weights until lettuce harvest in Exp_c. Overestimations of crop dry weight at harvest time
909 varied in all experiments. Exp_v1 showed the most significant overestimation, with an RMSE
910 of 0.0248 kg m⁻² (ground) in the last two samples. This was primarily induced by high
911 temperatures, which shortened the vegetative stage, triggering early bolting and stem elongation
912 (Hao et al., 2018; Rosental, Still, You, Hayes, & Simko, 2021). Although the *SLA* related
913 parameters were locally calibrated using the three sets of experimental data, including those
914 collected as stem elongated in the experiments, the adverse impact of stem elongation can only
915 be partially described. According to Eq. (9), the model assumes that shoot biomass is allocated
916 only to leaves. Once lettuce stems grow excessively, the model overestimates the change rate
917 in LAI and, thereby, crop dry weight. While this lettuce model is oriented towards the vegetative
918 stage with sufficient accuracy to meet control requirements, it may not fully explain the effects
919 of plant senescence. However, this limitation should not hinder its use in commercial
920 greenhouses, as growers will ensure timely harvesting based on daily observations to maintain
921 the quality and market value of the lettuce crop.

922 During the late stages of crop growth under high temperatures, the model overestimated LAI
923 (Fig. 10), consistent with the reasons for overestimating crop dry weight. Similarly, excluding
924 the last two samples in Exp_v1 reduced the RRMSE for LAI to 12.9%. Therefore, during the
925 vegetative growth stage concerned by commercial production, the model performed well in

926 simulating LAI dynamics, accurately predicting them with RRMSE ranging from 12.1% to
927 19.5%. While the LAI and biomass interact, as van Henten (1994a) found, their simulations
928 differed in estimations, including the timing and magnitude of deviations. These differences are
929 attributed to the model descriptions and samplings.

930

931 **4.2. The role of model framework and hypothesis**

932 The inhibitions across the three experiments demonstrate that the proposed model
933 framework and hypothesis worked in simulations (Fig. 11). Specifically, the model
934 supplements the canopy-level assimilation inhibition, going beyond the direct effects of
935 temperature on leaf photosynthesis and crop respiration. It particularly addresses the challenge
936 of quantifying growth inhibition by extremely low temperatures at night, which might be
937 reflected by the assimilation inhibition over the next few days. In essence, the instantaneous
938 extreme temperatures, whether during the day or night, achieve this inhibition by additionally
939 affecting potential growth rates and buffer flows, ultimately buffer evolution and canopy
940 photosynthesis. Without this inhibition, the lettuce growth model would severely overestimate
941 growth and present substantially poorer performance (Table 3). The overestimations were also
942 observed in our simulation tests of the one-state lettuce growth model proposed by van Henten
943 (1994a), using the experimental data from this study. These findings highlight the limitation of
944 existing models when applied to extreme environments.

945 In all three experiments, photosynthesis inhibition was lifted in the late stages of crop growth.
946 This is due to the increased dry matter. On one side, the outlet buffer flows called by potential
947 growth and maintenance respiration, along with buffer capacity, increase in proportion to crop
948 dry weight. However, on the other side, the canopy photosynthesis, as the source flows, does
949 not increase proportion to crop dry weight or LAI due to the limited light absorbed by the
950 canopy within a unit ground area. The cessation of inhibition partially explains the tendency of

951 the model to overestimate growth near harvest. In the calibration and two validation
 952 experiments, the crop dry weight leading to the complete disinhibition was 89.748×10^{-3} ,
 953 47.054×10^{-3} , and 77.737×10^{-3} kg m⁻² (ground), respectively. Higher temperatures resulted in
 954 shorter inhibition durations and lower crop dry weight required for complete disinhibition,
 955 indicating that the model shows greater tolerance to high-temperature stress than to low-
 956 temperature stress. This difference is further supported by the value of $T_{c,RGR}$, which was
 957 calibrated to be 25 °C.

958 A photosynthesis inhibition was observed during the initial stages of crop growth when the
 959 temperature is held constant at 25°C and does not contribute to the inhibition. The inhibition
 960 can occur despite buffer flows to growth conversion at the maximum achievable growth rate.
 961 This finding aligns with reality (Spitters et al., 1989), suggesting that the sink strength, instead
 962 of the photosynthesis with excess supply, dominates the initial crop growth and leaf area
 963 expansion. Thus, the hypothesis enables the model to effectively simulate early growth, which
 964 is not addressed by current models primarily focusing on the balance between photosynthesis
 965 and respiration. It should be mentioned that the model is sensitive to the parameter of $RGR_{max,20}$,
 966 according to the calibration process. We expect interested researchers to calibrate this parameter
 967 using additional data or further optimise the expression of RGR_{max} and explore the specific
 968 physiological implications.

969

970 Table 3 Performance comparison of the lettuce growth model with and without the proposed
 971 hypothesis of buffer evolution and canopy photosynthesis inhibition.

Indicators	Exp_v1	Exp_c	Exp_v2
Measured X_d at harvest [kg m ⁻² (ground)]	0.1506	0.1475	0.1953
Simulated X_d at harvest with hypothesis [kg m ⁻² (ground)]	0.1752	0.1649	0.2012

Simulated X_d at harvest without hypothesis [kg m ⁻² (ground)]	0.2536	0.2916	0.2998
RRMSE for X_d with hypothesis [%]	24.9	16.8	10.5
RRMSE for X_d without hypothesis [%]	142.7	177.0	109.0

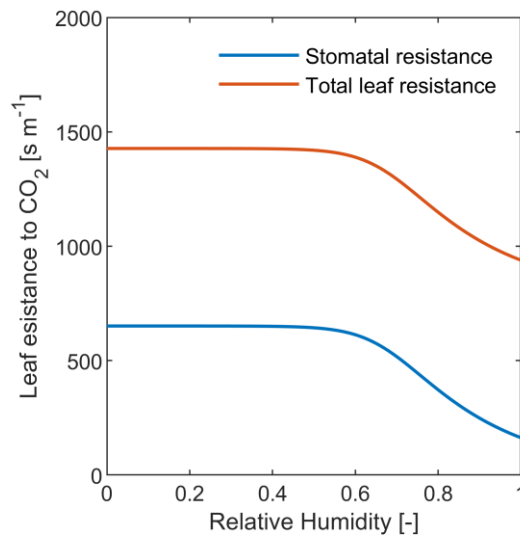
972

973 **4.3. Effects of humidity and specific leaf area**

974 In this model, air humidity affects lettuce growth from both biochemical and morphological
975 perspectives. As humidity increases, stomatal resistance and the total leaf resistance decrease
976 (Fig. 12), increasing the leaf photosynthesis rate. Concurrently, *SLA* increases along with the
977 increase in humidity (Fig. 6), promoting the leaf area expansion. Therefore, higher humidity
978 levels benefit canopy photosynthesis and dry matter accumulation. However, increasing
979 humidity may induce pest and disease issues and reduce transpiration (Stanghellini et al., 2019),
980 affecting water and nutrient uptake, both of which are not considered by the potential model of
981 this study.

982 The calibrated relative changes in *SLA* per unit changes of greenhouse climate imply the
983 same trend with literature (Bradbury & Ahmad, 1996; Carotti et al., 2021); increasing humidity
984 and decreasing radiation increase *SLA* of the lettuce. The inclusion of *SLA* enables the model
985 to describe the response of leaf morphogenesis to climate, which can improve modelling
986 accuracy. However, there is still much room for improvement in the *SLA* description,
987 considering that its goodness of fit ($R^2 = 0.380$, RMSE = 9.928) has not yet reached an ideal
988 state. Calibration using more data and modifying equation structure are the directions for
989 improvement.

990



991

992 Fig. 12 Leaf resistances to CO₂ diffusion as a function of T_c , X_h , X_c , and I , with $T_c = 25$ °C, X_c
 993 = $600 \mu\text{mol}(\text{CO}_2) \text{mol}^{-1}(\text{air})$, $I = 300 \text{ W m}^{-2}(\text{ground})$, and $LAI = 3 \text{ m}^2(\text{leaf}) \text{m}^{-2}(\text{ground})$.

994

995 4.4. Universality and limitations

996 The developed lettuce growth model belongs to the potential model category, only
 997 responding to the shoot environment inside the greenhouse. It has been demonstrated to respond
 998 to a broad range of greenhouse climates effectively and even works with sub-zero temperature
 999 inputs. The model accurately predicts dry matter and leaf area dynamics during growth stages
 1000 of interest in commercial lettuce production. Most knowledge of this process-based model can
 1001 be extended to other crops. Also, the model simulates instantaneous crop dynamics and shares
 1002 the same time scale as greenhouse climate models, allowing for the integrated description of
 1003 the greenhouse crop production process from external weather to crop biomass. These enable
 1004 the model to serve as a basis for optimal control of greenhouse climate, including those with
 1005 limited climate conditioning capabilities.

1006 One should recognise that crop models are essential for optimal climate control, particularly
 1007 when aiming to maximise net revenue or yield. However, they are rarely used independently
 1008 for control purposes; instead, they are typically integrated with greenhouse climate models to
 1009 simulate production processes and provide control signals. The lettuce model in this study is

1010 suited for control due to its mechanistic nature, offering computational efficiency and
1011 generalisation, along with design innovations that enhance prediction accuracy and
1012 compatibility with various greenhouse scenarios regarding indoor climate and cultivation.

1013 Lettuce growth follows the principle that the reciprocal of plant weight is linearly correlated
1014 with plant density (Scaife & Jones, 1976). In practice, however, an optimal planting density
1015 exists, which may vary depending on seasons and cultivars (Maboko & Du Plooy, 2009). To
1016 simplify modelling, the current mechanistic lettuce models do not explicitly incorporate density
1017 as an input but account for its influence through model calibration. For instance, the model by
1018 van Henten (1994a) was calibrated under a planting density of 18 plants m⁻², while the model
1019 by Pearson et al. (1997) used 25 plants m⁻². Similarly, in our model, the input of plant density
1020 is used only to determine individual plant dry weight, and the effects of density are implicitly
1021 included by model evaluation under a density of approximately 11.5 plants m⁻². However, our
1022 model defaults to an effective cultivation area-based plant density, where each lettuce plant
1023 occupies a limited ground area at maximum. The plant density is crucial for determining initial
1024 crop states and root ratio, and accurately predicting biomass and yield within the greenhouse or
1025 a specific area together with the counted effective cultivation area. Importantly, this study
1026 represents the first instance of defining the density basis for the lettuce model, enabling its
1027 application across both high- and low-density planting scenarios. This adaptability is
1028 particularly significant for implementing optimal control strategies in practical greenhouse
1029 systems, where not all ground area is used for cultivation.

1030 The climate inputs for model evaluation, derived from low-tech greenhouses, include air
1031 temperature and humidity with extreme values, solar radiation passing through plastic film, and
1032 CO₂ concentration under natural ventilation. However, in modern multi-span greenhouses, CO₂
1033 concentration is usually maintained at 700-1000 μmol mol⁻¹ during photosynthesis through CO₂
1034 supplementation. This study lacks model validation under such high CO₂ concentrations. The

1035 description of stomatal conductance adopts the parameters given by Stangheilini (1987) for
1036 tomatoes, and subsequent research is needed to determine these parameters for lettuce. Using
1037 the experimental data from this study, the one-state model by van Henten (1994a) significantly
1038 overestimated growth predictions. Possible reasons include the imposed constraints on
1039 temperature inputs, as well as the influence of different cultivation practices where the Eldert
1040 model was developed for soilless cultivation while lettuce was grown in soil in our experiments.
1041 Inspired by these findings, we also expect interested researchers and technicians to conduct
1042 model evaluation or parameter calibration for soilless cultivation scenarios and other varieties.
1043 Furthermore, we leave the sub-model validation and further exploration of the proposed
1044 photosynthesis inhibition hypothesis to botanists. To explain the effects of lettuce plant
1045 senescence and enhance prediction accuracy, thermal time or chronological time could be
1046 introduced to characterise the decline in photosynthetic capacity with plant age, as suggested
1047 by Sweeney et al. (1981) and Pearson et al. (1997).

1048 To use the developed model, the following preparations are necessary:

- 1049 • Providing model inputs, including greenhouse climate data (shortwave radiation I , air
1050 temperature X_t , humidity X_h , and CO₂ concentration X_c) and initial value of crop states
1051 (crop dry weight X_d , LAI , and buffer storage C_{buf}).
- 1052 • Identifying the recovering period, after which simulations can be performed.
- 1053 • Counting the effective cultivated area and determining plant density ρ_c .

1054

1055 **5. Conclusion**

1056 In this study, a lettuce growth model that describes the effects of a broad range of greenhouse
1057 climates on crop dry weight dynamics was developed, calibrated, and validated. The developed
1058 model is for optimal climate control purposes. It simulates instantaneous crop dynamics for the
1059 potential situation. The greenhouse climates considered by the model include air temperature

1060 with extremely low and high conditions, humidity, CO₂ concentration, and shortwave radiation.
1061 The model defaults to an effective cultivated area-based plant density, where a single plant
1062 occupies a limited ground area at maximum, making the model universal.

1063 The model development focused on extending crop growth responses to extreme
1064 temperatures and humidity. The model framework performs two parallel sets of mass flows:
1065 dry matter accumulation and buffer evolution. They share paths but differ in logic. The former
1066 processes contribute to crop growth, where the carbohydrates produced by canopy
1067 photosynthesis are partly consumed in maintenance respiration, and the remaining are
1068 converted into structural dry matter and partitioned among organs. The latter processes are used
1069 to manage growth inhibition partly induced by adverse temperatures through regulating canopy
1070 photosynthesis. The buffer carbohydrates flow to growth conversion based on the temperature-
1071 dependent maximum growth rate (sink strength) of the whole crop. As extreme temperatures,
1072 both during the day and night, inhibit the partitioning, buffer storage may not be consumed
1073 promptly, and the canopy assimilation inhibition occurs when the storage reaches the buffer
1074 capacity. Humidity effects are quantified by describing stomatal resistance and the SLA of new
1075 leaves. In addition, for simplicity, leaf carboxylation resistance and root ratio are described as
1076 descriptive functions.

1077 The model performance was demonstrated to be good and acceptable for a broad range of
1078 greenhouse climates. The simulated dry matter weights closely mirrored the measured values,
1079 with the RRMSE of 10.5-24.9% and the RMSE of 0.0070-0.0131 kg m⁻². The model predicted
1080 the LAI dynamics with an RRMSE of 12.1-54.7%. However, during the vegetative growth stage
1081 relevant to commercial production, it performed well in LAI prediction, with an RRMSE
1082 ranging from 12.1% to 19.5%. The proposed model framework and underlying hypothesis
1083 worked in simulations that the photosynthesis inhibition time accounted for 27-41% of the total
1084 photosynthesis time. They adequately characterise the effects of greenhouse air temperature,

1085 including extreme conditions, on crop growth and enable the model to simulate early growth.
1086 Inhibition was lifted in the late stages of crop growth due to the increased dry matter. Moreover,
1087 the model showed greater tolerance to high-temperature than low-temperature stress. Higher
1088 humidity levels benefit canopy photosynthesis by decreasing stomatal resistance and increasing
1089 the SLA of new leaves.

1090 The model can serve as a basis for optimal management of greenhouse climate, including
1091 those with limited climate conditioning capabilities. The simulation requires model inputs of
1092 greenhouse climate, initial crop states, and plant density, and needs to identify the recovering
1093 period. Further study is expected to validate the model for more lettuce cultivation scenarios
1094 and introduce the effects of lettuce plant senescence.

1095

1096 **Data availability**

1097 The raw data that support the findings of this study are openly available at Mendeley Data,
1098 <http://dx.doi.org/10.17632/r7z9ttvkyh.2>.

1099

1100 **Acknowledgement**

1101 This research was supported by the Special Innovation Ability Construction Fund of Beijing
1102 Academy of Agriculture and Forestry Sciences [grant number KJCX20240405]; joint
1103 Innovate UK, UK-China: precision for enhancing agricultural productivity project [grant
1104 number 107459]; and the Key Research and Development Project of Shandong Province,
1105 China [grant number 2022CXGC020708-4]. The authors would like to thank Daniel Reyes
1106 Lastiri and Simon van Mourik from Wageningen University for their guidance and
1107 suggestions at the early stage of formulating this manuscript. We also thank Lichun Wang
1108 greatly for his help with lettuce cultivation experiments.

1109

1110 **Appendix A. Model smoothing**

1111

1112 In Section 2.2.2, the model equations are not entirely written in a continuously differentiable
 1113 form, considering that the model is not only used for control and that not all optimisation
 1114 control algorithms require continuous differentiability. For instance, genetic algorithms and
 1115 particle swarm optimisation algorithms do not need it. Thus, the equations were presented in
 1116 their original form. However, model smoothing, particularly implemented for conditional
 1117 statements using switch functions, can speed up simulations and ensure that gradient-based
 1118 optimisation algorithms can be applied to control systems based on this model. To improve
 1119 the generalisability of the model, Eq. (2), (3), (26), (27), (31), and (32) can be smoothed as
 1120 follows:

1121

$$\begin{aligned}
 h_{buf} = & \left(\frac{1}{1 + e^{-s_{h,buf,1} \cdot \left(\frac{C_{buf}}{C_{buf,max}} - 0.99 \right)}} \right) \cdot \frac{-1}{s_{h,buf,2}} \\
 & \cdot \ln \left(e^{-s_{h,buf,2} \cdot \frac{R_d + \frac{RGR_{max} \cdot X_d}{c_\beta}}{c_\alpha \cdot (A_C + z_{h,buf})}} + e^{-s_{h,buf,2}} \right) \\
 & + \left(1 - \frac{1}{1 + e^{-s_{h,buf,1} \cdot \left(\frac{C_{buf}}{C_{buf,max}} - 0.99 \right)}} \right) \cdot 1
 \end{aligned} \tag{A1}$$

1122

$$\begin{aligned}
 RGR_{max} = & \left(\frac{1}{1 + e^{-s_{RGR,max} \cdot (T_c - T_{c,RGR})}} \right) \cdot RGR_{max,20} \cdot Q_{10,gr}^{\frac{T_c - 20}{10}} \\
 & + \left(1 - \frac{1}{1 + e^{-s_{RGR,max} \cdot (T_c - T_{c,RGR})}} \right) \cdot RGR_{max,20} \cdot Q_{10,gr}^{\frac{T_c - 20}{10}}
 \end{aligned} \tag{A2}$$

1123

$$f_{T_c,s} = \left(\frac{1}{1 + e^{-s_{f,T_c,s} \cdot (I-3)}} \right) \cdot (1 + 2.3 \cdot 10^{-2} \cdot (T_c - 24.5)^2) \\ + \left(1 - \frac{1}{1 + e^{-s_{f,T_c,s} \cdot (I-3)}} \right) \cdot (1 + 0.5 \cdot 10^{-2} \cdot (T_c - 33.6)^2) \quad (\text{A3})$$

1124

$$f_{X_c,s} = \left(\frac{1}{1 + e^{-s_{f,X_c,s,1} \cdot (I-3)}} \right) \\ \cdot \left(\left(\frac{1}{1 + e^{-s_{f,X_c,s,2} \cdot (X_c - 1100)}} \right) \cdot 1.5 + \left(1 - \frac{1}{1 + e^{-s_{f,X_c,s,2} \cdot (X_c - 1100)}} \right) \right) \\ \cdot (1 + 6.1 \cdot 10^{-7} \cdot (X_c - 200)^2) + \left(1 - \frac{1}{1 + e^{-s_{f,X_c,s,1} \cdot (I-3)}} \right) \cdot 1 \quad (\text{A4})$$

1125

$$e_{s,air} = \left(\frac{1}{1 + e^{-s_{e,s,air} \cdot X_t}} \right) \cdot 10^{2.7857 + \frac{7.5 \cdot X_t}{237.3 + X_t}} + \left(1 - \frac{1}{1 + e^{-s_{e,s,air} \cdot X_t}} \right) \\ \cdot 10^{2.7857 + \frac{9.5 \cdot X_t}{265.5 + X_t}} \quad (\text{A5})$$

1126

$$r_b = Le^{0.67} \cdot \frac{1174 \cdot l_f^{0.5}}{\left(l_f \cdot ((T_c - X_t)^2 + z_{r,b}^2) \right)^{0.5} + 207 \cdot v_a^2} \quad (\text{A6})$$

1127

1128 The slope of the differentiable switch function for each model equation might be different,
 1129 primarily depending on the desired range of input variables over which the model description
 1130 intends the switch function to complete the transition between 0 and 1. For model smoothing,
 1131 all introduced parameters, and their values are summarised in Table A1. In Eq. (A1), the
 1132 threshold of 0.99 was defined to ensure that the calculation of h_{buf} could be based entirely on
 1133 the formula applicable when $C_{buf} = C_{buf,max}$. As an example, the patterns of the switching
 1134 function and the smooth minimum for h_{buf} are depicted in Fig. A1. No obvious differences
 1135 were found between the simulation results of the smoothed lettuce growth model and the

1136 original model. Readers can decide whether to apply the smoothing process based on specific
 1137 needs. The code for the smoothed model is available at
 1138 <http://dx.doi.org/10.17632/r7z9ttvkyh.2>.

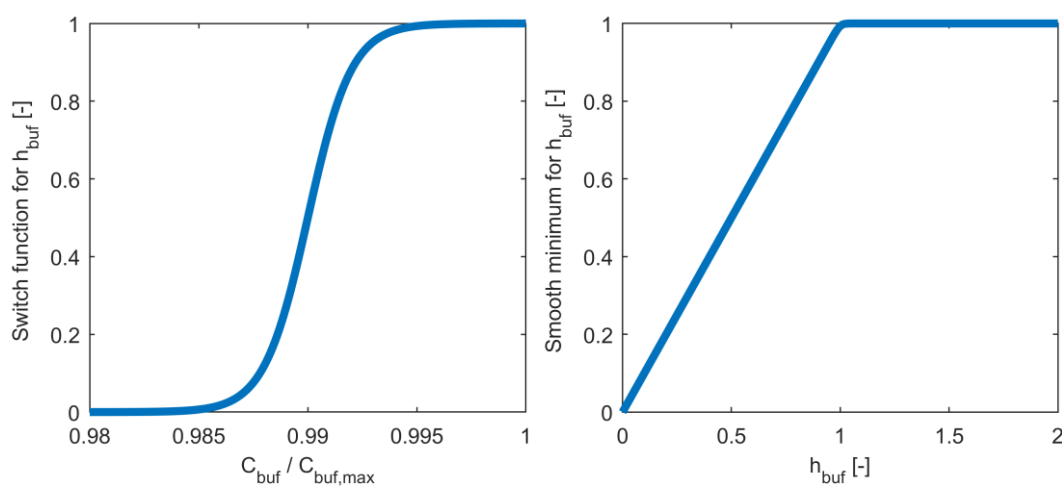
1139

1140 Table A1 Introduced parameters for smoothing the lettuce growth model

1141

Notation	Meaning	Value	Unit
$S_{h,buf,1}$	Slope of the differentiable switch function for h_{buf}	1000	-
$S_{h,buf,2}$	Sharpness parameter of the smooth minimum for h_{buf}	100	-
$z_{h,buf}$	Auxiliary parameter to prevent A_C from being zero in the denominator of h_{buf}	1×10^{-12}	kg (CO ₂) m ⁻² (ground) s ⁻¹
$S_{RGR,max}$	Slope of the differentiable switch function for RGR_{max}	10	°C ⁻¹
$S_{f,Tc,s}$	Slope of the differentiable switch function for $f_{Tc,s}$	10	m ² (ground) W ⁻¹
$S_{f,Xc,s,1}$	Slope of the radiation dependent differentiable switch function for $f_{Xc,s}$	10	m ² (ground) W ⁻¹
$S_{f,Xc,s,2}$	Slope of the CO ₂ dependent differentiable switch function for $f_{Xc,s}$	0.5	(μmol (CO ₂) mol ⁻¹ (air)) ⁻¹
$S_{e,s,air}$	Slope of the differentiable switch function for $e_{s,air}$	10	°C ⁻¹
$z_{r,b}$	Auxiliary parameter to smooth the absolute value function for r_b	1×10^{-4}	°C

1142



1143

1144 **Fig. A1** Curve patterns of the smoothing functions for the buffer dependent inhibition
1145 function (h_{buf}).

1146

1147 **References**

1148

1149 Bakker, J. C. (1991). Analysis of humidity effects on growth and production of glasshouse fruit vegetables.

1150 Wageningen University and Research, The Netherlands.

1151 Bakker, J. C., Bot, G. P. A., Challa, H., & van de Braak, N. J. (1995). Greenhouse climate control: an integrated

1152 approach. Wageningen: Wageningen Academic Publishers.

1153 Bot, G. P. A. (1983). Greenhouse climate: from physical processes to a dynamic model. Wageningen University

1154 and Research, The Netherlands.

1155 Bradbury, M., & Ahmad, R. (1996). Effect of humidity on growth of lettuce (*Lactuca sativa*, var. Great Lakes)

1156 under saline condition. *Pakistan Journal of Botany*, 28(1), 97-102.

1157 Carini, F., Cargnelutti Filho, A., Bandeira, C. T., Neu, I. M. M., Pezzini, R. V., Pacheco, M., & Tomasi, R. M.

1158 (2019). Growth models for lettuce cultivars growing in spring. *Journal of Agricultural Science*, 11, 147-

1159 159. <https://doi.org/10.5539/jas.v11n6p147>

1160 Carotti, L., Graamans, L., Puksic, F., Butturini, M., Meinen, E., Heuvelink, E., & Stanghellini, C. (2021). Plant

1161 factories are heating up: Hunting for the best combination of light intensity, air temperature and root-

1162 zone temperature in lettuce production. *Frontiers in Plant Science*, 11, 592171.

1163 <https://doi.org/10.3389/fpls.2020.592171>

1164 Chalabi, Z. S., Biro, A., Bailey, B. J., Aikman, D. P., & Cockshull, K. E. (2002). Optimal control strategies for

1165 carbon dioxide enrichment in greenhouse tomato crops - Part 1: Using pure carbon dioxide. *Biosystems*

1166 *Engineering*, 81(4), 421-431. <https://doi.org/10.1006/bioe.2001.0039>

1167 Chang, C.-L., Chung, S.-C., Fu, W.-L., & Huang, C.-C. (2021). Artificial intelligence approaches to predict

1168 growth, harvest day, and quality of lettuce (*Lactuca sativa* L.) in a IoT-enabled greenhouse system.

1169 *Biosystems Engineering*, 212, 77-105. <https://doi.org/10.1016/j.biosystemseng.2021.09.015>

1170 Collier, G. F., & Tibbitts, T. W. (1984). Effects of relative humidity and root temperature on calcium

1171 concentration and tipburn development in lettuce. *Journal of the American Society for Horticultural*

1172 *Science*, 109(2), 128-131. <https://doi.org/10.21273/JASHS.109.2.128>

1173 Critten, D. L. (1991). Optimization of CO₂ concentration in greenhouses: A modelling analysis for the lettuce
1174 crop. *Journal of Agricultural Engineering Research*, 48, 261-271. <https://doi.org/10.1016/0021->
1175 8634(91)80020-F

1176 Dayan, E., van Keulen, H., Jones, J. W., Zipori, I., Shmuel, D., & Challa, H. (1993a). Development, calibration
1177 and validation of a greenhouse tomato growth model: I. Description of the model. *Agricultural Systems*,
1178 43(2), 145-163. [https://doi.org/10.1016/0308-521X\(93\)90024-V](https://doi.org/10.1016/0308-521X(93)90024-V)

1179 Dayan, E., van Keulen, H., Jones, J. W., Zipori, I., Shmuel, D., & Challa, H. (1993b). Development, calibration
1180 and validation of a greenhouse tomato growth model: II. Field calibration and validation. *Agricultural*
1181 *Systems*, 43(2), 165-183. [https://doi.org/10.1016/0308-521X\(93\)90025-W](https://doi.org/10.1016/0308-521X(93)90025-W)

1182 Farquhar, G. D., von Caemmerer, S., & Berry, J. A. (1980). A biochemical model of photosynthetic CO₂
1183 assimilation in leaves of C₃ species. *Planta*, 149(1), 78-90. <https://doi.org/10.1007/BF00386231>

1184 Gary, C., Barczi, J. F., Bertin, N., & Tchamitchian, M. (1994). Simulation of individual organ growth and
1185 development on a tomato plant: a model and a user-friendly interface. Paper presented at the
1186 Greenhouse Environment Control and Automation. <https://doi.org/10.17660/ActaHortic.1995.399.23>

1187 Gijzen, H., Heuvelink, E., Challa, H., Marcelis, L. F. M., Dayan, E., Cohen, S., & Fuchs, M. (1997).
1188 HORTISIM: a model for greenhouse crops and greenhouse climate. Paper presented at the II Modelling
1189 Plant Growth, Environmental Control and Farm Management in Protected Cultivation.
1190 <https://doi.org/10.17660/ActaHortic.1998.456.53>

1191 Goudriaan, J. (1982). Potential production processes. In F. W. T. Penning de Vries & H. H. van Laar (Eds.),
1192 Simulation of plant growth and crop production (pp. 98-113). Wageningen: Pudoc.

1193 Goudriaan, J. (1986). A simple and fast numerical method for the computation of daily totals of crop
1194 photosynthesis. *Agricultural and Forest Meteorology*, 38, 249-254. <https://doi.org/10.1016/0168->
1195 1923(86)90063-8

1196 Goudriaan, J., & van Laar, H. H. (1994). *Modelling Potential Crop Growth Processes*. The Netherlands: Kluwer
1197 Academic Publishers.

1198 Goudriaan, J., van Laar, H. H., van Keulen, H., & Louwarse, W. (1985). Photosynthesis, CO₂ and plant
1199 production. In W. Day & R. K. Atkin (Eds.), *Wheat growth and modelling* (pp. 107-122): Springer.

1200 Hao, J., Zhang, L., Li, P., Sun, Y., Li, J., Qin, X., . . . Han, Y. (2018). Quantitative proteomics analysis of lettuce
1201 (*Lactuca sativa* L.) reveals molecular basis-associated auxin and photosynthesis with bolting induced by

1202 high temperature. *International Journal of Molecular Sciences*, 19(10), 2967.
1203 <https://doi.org/10.3390/ijms19102967>

1204 Ioslovich, I. (2009). Optimal control strategy for greenhouse lettuce: Incorporating supplemental lighting.
1205 *Biosystems Engineering*, 103(1), 57-67. <https://doi.org/10.1016/j.biosystemseng.2009.01.015>

1206 Ioslovich, I., Moran, M. I. R. S., & Gutman, P. (2005). Nonlinear Dynamic Lettuce Growth Model: Parameter
1207 Selection and Estimation for N-Limited Experiments. Paper presented at the Proceedings of the 44th
1208 IEEE Conference on Decision and Control.

1209 Jamieson, P. D., Porter, J. R., & Wilson, D. R. (1991). A test of the computer simulation model ARCWHEAT1
1210 on wheat crops grown in New Zealand. *Field Crops Research*, 27(4), 337-350.
1211 [https://doi.org/10.1016/0378-4290\(91\)90040-3](https://doi.org/10.1016/0378-4290(91)90040-3)

1212 Jones, J. W., Dayan, E., Allen, L. H., van Keulen, H., & Challa, H. (1991). A dynamic tomato growth and yield
1213 model (TOMGRO). *Transactions of the ASAE*, 34(2), 663-672. <https://doi.org/10.13031/2013.31715>

1214 Katzin, D., van Henten, E. J., & van Mourik, S. (2022). Process-based greenhouse climate models: Genealogy,
1215 current status, and future directions. *Agricultural Systems*, 198, 103388.
1216 <https://doi.org/10.1016/j.agsy.2022.103388>

1217 Körner, O., & van Straten, G. (2008). Decision support for dynamic greenhouse climate control strategies.
1218 *Computers and Electronics in Agriculture*, 60(1), 18-30. <https://doi.org/10.1016/j.compag.2007.05.005>

1219 Kuijpers, W. J., Antunes, D. J., van Mourik, S., van Henten, E. J., & van de Molengraft, M. J. G. (2022).
1220 Weather forecast error modelling and performance analysis of automatic greenhouse climate control.
1221 *Biosystems Engineering*, 214, 207-229. <https://doi.org/10.1016/j.biosystemseng.2021.12.014>

1222 Lazof, D. B., Bernstein, N., & Läuchli, A. (1991). Growth and development of the *Lactuca sativa* shoot as
1223 affected by NaCl stress: consideration of leaf developmental stages. *Botanical Gazette*, 152(1), 72-76.
1224 <https://www.jstor.org/stable/2995493>

1225 Li, Q., Gao, H., Zhang, X., Ni, J., & Mao, H. (2022). Describing Lettuce Growth Using Morphological Features
1226 Combined with Nonlinear Models. *Agronomy*, 12(4), 860. <https://doi.org/10.3390/agronomy12040860>

1227 Maboko, M. M., & Du Plooy, C. P. (2009). Effect of plant spacing on growth and yield of lettuce (*Lactuca sativa*
1228 L.) in a soilless production system. *South African Journal of Plant and Soil*, 26(3), 195-198.
1229 <https://doi.org/10.1080/02571862.2009.10639954>

1230 Marcelis, L. F. M. (1996). Sink strength as a determinant of dry matter partitioning in the whole plant. *Journal of*
1231 *experimental botany*, 47(Special Issue), 1281-1291. https://doi.org/10.1093/jxb/47.Special_Issue.1281

1232 Marcelis, L. F. M., Heuvelink, E., & Goudriaan, J. (1998). Modelling biomass production and yield of
1233 horticultural crops: a review. *Scientia Horticulturae*, 74, 83-111. <https://doi.org/10.1016/S0304->
1234 [4238\(98\)00083-1](https://doi.org/10.1016/S0304-4238(98)00083-1)

1235 Mathieu, J., Linker, R., Levine, L., Albright, L., Both, A. J., Spanswick, R., . . . Langhans, R. (2006). Evaluation
1236 of the Nicolet model for simulation of short-term hydroponic lettuce growth and nitrate uptake.
1237 *Biosystems engineering*, 95(3), 323-337. <https://doi.org/10.1016/j.biosystemseng.2006.07.006>

1238 Mohamed, G., Heynes, X., Naser, A., Sun, W., Hardy, K., Grundy, S., & Lu, C. (2023). Modelling daily plant
1239 growth response to environmental conditions in Chinese solar greenhouse using Bayesian neural
1240 network. *Scientific Reports*, 13(1), 4379. <https://doi.org/10.1038/s41598-023-30846-y>

1241 Mokhtar, A., El-Ssawy, W., He, H., Al-Anasari, N., Sammen, S. S., Gyasi-Agyei, Y., & Abuarab, M. (2022).
1242 Using machine learning models to predict hydroponically grown lettuce yield. *Frontiers in Plant*
1243 *Science*, 13, 706042. <https://doi.org/10.3389/fpls.2022.706042>

1244 Monteith, J. L. (1995). A reinterpretation of stomatal responses to humidity. *Plant, Cell & Environment*, 18(4),
1245 357-364. <https://doi.org/10.1111/j.1365-3040.1995.tb00371.x>

1246 Monteith, J. L., & Unsworth, M. H. (2013). *Principles of environmental physics: plants, animals, and the*
1247 *atmosphere* (4th ed.). Oxford: Academic Press.

1248 Mortensen, L. M. (1986). Effect of relative humidity on growth and flowering of some greenhouse plants.
1249 *Scientia Horticulturae*, 29(4), 301-307. [https://doi.org/10.1016/0304-4238\(86\)90013-0](https://doi.org/10.1016/0304-4238(86)90013-0)

1250 Pearson, S., Wheeler, T. R., Hadley, P., & Wheldon, A. E. (1997). A validated model to predict the effects of
1251 environment on the growth of lettuce (*Lactuca sativa* L.): implications for climate change. *Journal of*
1252 *Horticultural Science*, 72(4), 503-517. <https://doi.org/10.1080/14620316.1997.11515538>

1253 Penning De Vries, F. W. T., & van Laar, H. H. (1982). Simulation of growth processes and the model BACROS.
1254 In F. W. T. Penning de Vries & H. H. van Laar (Eds.), *Simulation of plant growth and crop production*
1255 (pp. 114-135). Wageningen: Pudoc.

1256 Rahimikhoob, H., Delshad, M., & Habibi, R. (2023). Leaf area estimation in lettuce: Comparison of artificial
1257 intelligence-based methods with image analysis technique. *Measurement*, 222, 113636.
1258 <https://doi.org/10.1016/j.measurement.2023.113636>

1259 Rawson, H. M., Begg, J. E., & Woodward, R. G. (1977). The effect of atmospheric humidity on photosynthesis,
1260 transpiration and water use efficiency of leaves of several plant species. *Planta*, 134(1), 5-10.
1261 <https://doi.org/10.1007/BF00390086>

- 1262 Rohde, W., & Forni, F. (2023). Lettuce modelling for growth control in precision agriculture. *European Journal*
1263 *of Control*, 74, 100843. <https://doi.org/10.1016/j.ejcon.2023.100843>
- 1264 Rosental, L., Still, D. W., You, Y., Hayes, R. J., & Simko, I. (2021). Mapping and identification of genetic loci
1265 affecting earliness of bolting and flowering in lettuce. *Theoretical and Applied Genetics*, 134(10), 3319-
1266 3337. <https://doi.org/10.1007/s00122-021-03898-9>
- 1267 Scaife, M. A., & Jones, D. (1976). The relationship between crop yield (or mean plant weight) of lettuce and
1268 plant density, length of growing period, and initial plant weight. *The Journal of Agricultural Science*,
1269 86(1), 83-91. <https://doi.org/10.1017/S002185960006500X>
- 1270 Schuepp, P. H. (1993). Tansley review No. 59. Leaf boundary layers. *New Phytologist*, 125, 477-507.
1271 <https://www.jstor.org/stable/2558258>
- 1272 Seginer, I. (2003). A dynamic model for nitrogen-stressed lettuce. *Annals of Botany*, 91(6), 623-635.
1273 <https://doi.org/10.1093/aob/mcg069>
- 1274 Seginer, I., Buwalda, F., & van Straten, G. (1999). Lettuce growth limited by nitrate supply. Paper presented at
1275 the III International Workshop on Models for Plant Growth and Control of the Shoot and Root
1276 Environments in Greenhouses. <https://doi.org/10.17660/ActaHortic.1999.507.16>
- 1277 Seginer, I., Linker, R., Buwalda, F., van Straten, G., & Bleyaert, P. (2003). The NICOLET lettuce model: a
1278 theme with variations. Paper presented at the International Workshop on Models for Plant Growth and
1279 Control of Product Quality in Horticultural Production 654.
- 1280 Seginer, I., Shina, G., Albright, L. D., & Marsh, L. S. (1991). Optimal temperature setpoints for greenhouse
1281 lettuce. *Journal of Agricultural Engineering Research*, 49, 209-226. [https://doi.org/10.1016/0021-](https://doi.org/10.1016/0021-8634(91)80040-L)
1282 [8634\(91\)80040-L](https://doi.org/10.1016/0021-8634(91)80040-L)
- 1283 Seginer, I., van Straten, G., & Buwalda, F. (1998). Nitrate concentration in greenhouse lettuce: a modeling study.
1284 Paper presented at the II Modelling Plant Growth, Environmental Control and Farm Management in
1285 Protected Cultivation. <https://doi.org/10.17660/ActaHortic.1998.456.21>
- 1286 Shimizu, H., Kushida, M., & Fujinuma, W. (2008). A growth model for leaf lettuce under greenhouse
1287 environments. *Environmental Control in Biology*, 46(4), 211-219. <https://doi.org/10.2525/ecb.46.211>
- 1288 Sinclair, T. R., & Seligman, N. a. (2000). Criteria for publishing papers on crop modeling. *Field Crops Research*,
1289 68(3), 165-172. [https://doi.org/10.1016/S0378-4290\(00\)00105-2](https://doi.org/10.1016/S0378-4290(00)00105-2)

- 1290 Spitters, C. J. T., van Keulen, H., & van Kraalingen, D. W. G. (1989). A simple and universal crop growth
1291 simulator: SUCROS87. In R. Rabbinge, S. A. Ward & H. H. van Laar (Eds.), *Simulation and systems
1292 management in crop protection* (pp. 147-181). Wageningen: Pudoc.
- 1293 Stanghellini, C. (1987). *TRANSPARATION OF GREENHOUSE CROPS: an aid to climate management*.
1294 Wageningen University and Research, The Netherlands.
- 1295 Stanghellini, C., van't Oosfer, B., & Heuvelink, E. (2019). *Greenhouse horticulture: technology for optimal crop
1296 production*. Wageningen: Wageningen Academic Publishers.
- 1297 Stützel, H., & Chen, T. (2020). *5 Models of Vegetable Growth and Development* (Vol. 10).
- 1298 Sun, W., Guo, W., Xu, F., Wang, L., Xue, X., Li, Y., & Chen, Y. (2015). Application effect of surplus air heat
1299 pump heating system in Chinese solar greenhouse. *Transactions of the Chinese Society of Agricultural
1300 Engineering*, 31(17), 235-243. <https://doi.org/10.11975/j.issn.1002-6819.2015.17.031>
- 1301 Sweeney, D. G., Hand, D. W., Slack, G., & Thornley, J. H. M. (1981). Modelling the growth of winter lettuce.
1302 *Mathematics and plant physiology*, 217-229.
- 1303 Talbot, M.-H., & Monfet, D. (2024). Development of a crop growth model for the energy analysis of controlled
1304 agriculture environment spaces. *Biosystems Engineering*, 238, 38-50.
1305 <https://doi.org/10.1016/j.biosystemseng.2023.12.012>
- 1306 Tap, F. (2000). *Economics-based optimal control of greenhouse tomato crop production*. Wageningen University
1307 and Research, The Netherlands.
- 1308 Tei, F., Aikman, D. P., & Scaife, A. (1996). Growth of lettuce, onion and red beet. 2. Growth modelling. *Annals
1309 of Botany*, 78(5), 645-652.
- 1310 Thompson, H. C., Langhans, R. W., Both, A.-J., & Albright, L. D. (1998). Shoot and root temperature effects on
1311 lettuce growth in a floating hydroponic system. *Journal of the American Society for Horticultural
1312 Science*, 123(3), 361-364. <https://doi.org/10.21273/JASHS.123.3.361>
- 1313 Thornley, J. H. M., & Hurd, R. G. (1974). An analysis of the growth of young tomato plants in water culture at
1314 different light integrals and CO₂ concentrations: II. A mathematical model. *Annals of Botany*, 38(2),
1315 389-400. <https://doi.org/10.1093/oxfordjournals.aob.a084822>
- 1316 Tibbitts, T. W., & Bottenberg, G. (1976). Growth of lettuce under controlled humidity levels. *Journal of the
1317 American Society for Horticultural Science*, 101(1), 70-73. <https://doi.org/10.21273/JASHS.101.1.70>

1318 van Beveren, P. J. M., Bontsema, J., van Straten, G., & van Henten, E. J. (2015). Optimal control of greenhouse
1319 climate using minimal energy and grower defined bounds. *Applied Energy*, 159, 509-519.
1320 <https://doi.org/10.1016/j.apenergy.2015.09.012>

1321 van Henten, E. J. (1994a). *Greenhouse climate management: an optimal control approach*. Wageningen
1322 University and Research, The Netherlands.

1323 van Henten, E. J. (1994b). Validation of a dynamic lettuce growth model for greenhouse climate control.
1324 *Agricultural Systems*, 45(1), 55-72. [https://doi.org/10.1016/S0308-521X\(94\)90280-1](https://doi.org/10.1016/S0308-521X(94)90280-1)

1325 van Henten, E. J. (2003). Sensitivity analysis of an optimal control problem in greenhouse climate management.
1326 *Biosystems Engineering*, 85(3), 355-364. [https://doi.org/10.1016/s1537-5110\(03\)00068-0](https://doi.org/10.1016/s1537-5110(03)00068-0)

1327 van Holsteijn, H. M. C. (1980). *Growth of lettuce: Quantitative analysis of growth*: Veenman.

1328 van Keulen, H., Penning de Vries, F. W. T., & Drees, E. M. (1982). A summary model for crop growth. In F. W.
1329 T. Penning de Vries & H. H. van Laar (Eds.), *Simulation of plant growth and crop production* (pp. 87-
1330 97). Wageningen: Pudoc.

1331 van Laar, H. H., Goudriaan, J., & van Keulen, H. (1997). *SUCROS97: Simulation of crop growth for potential
1332 and water-limited production situations. As applied to spring wheat*. Wageningen: AB-DLO, TPE.

1333 van Ooteghem, R. J. C. (2010). *Optimal control design for a solar greenhouse*. Wageningen University and
1334 Research, The Netherlands.

1335 van Ploeg, D., & Heuvelink, E. (2005). Influence of sub-optimal temperature on tomato growth and yield: a
1336 review. *The Journal of Horticultural Science and Biotechnology*, 80(6), 652-659.
1337 <https://doi.org/10.1080/14620316.2005.11511994>

1338 van Straten, G., Challa, H., & Buwalda, F. (2000). Towards user accepted optimal control of greenhouse climate.
1339 *Computers and Electronics in Agriculture*, 26(3), 221-238. [https://doi.org/10.1016/S0168-
1340 1699\(00\)00077-6](https://doi.org/10.1016/S0168-1699(00)00077-6)

1341 van Straten, G., van Willigenburg, G., van Henten, E., & van Ooteghem, R. (2010). *Optimal control of
1342 greenhouse cultivation*. Boca Raton: CRC Press.

1343 Vanthoor, B. H. E. (2011). *A model-based greenhouse design method*. Wageningen University and Research,
1344 The Netherlands.

1345 Vanthoor, B. H. E., De Visser, P. H. B., Stanghellini, C., & van Henten, E. J. (2011). A methodology for model-
1346 based greenhouse design: Part 2, description and validation of a tomato yield model. *Biosystems
1347 engineering*, 110(4), 378-395. <https://doi.org/10.1016/j.biosystemseng.2011.08.005>

1348 Vanthoor, B. H. E., Stanghellini, C., van Henten, E. J., & De Visser, P. H. B. (2011). A methodology for model-
1349 based greenhouse design: Part 1, a greenhouse climate model for a broad range of designs and climates.
1350 *Biosystems Engineering*, 110(4), 363-377. <https://doi.org/10.1016/j.biosystemseng.2011.06.001>

1351 Volente, G. (2022). Lettuce temperature tolerance, 2024, from [https://www.greenhousetoday.com/lettuce-
1352 temperature-tolerance/](https://www.greenhousetoday.com/lettuce-temperature-tolerance/)

1353 Xu, D., Du, S., & van Willigenburg, G. (2018). Adaptive two time-scale receding horizon optimal control for
1354 greenhouse lettuce cultivation. *Computers and Electronics in Agriculture*, 146, 93-103.
1355 <https://doi.org/10.1016/j.compag.2018.02.001>

1356 Xu, D., Du, S., & van Willigenburg, G. (2019). Double closed-loop optimal control of greenhouse cultivation.
1357 *Control Engineering Practice*, 85, 90-99. <https://doi.org/10.1016/j.conengprac.2019.01.010>

1358 Xu, D., Du, S., & van Willigenburg, L. G. (2018). Optimal control of Chinese solar greenhouse cultivation.
1359 *Biosystems Engineering*, 171, 205-219. <https://doi.org/10.1016/j.biosystemseng.2018.05.002>

1360 Yin, X., & van Laar, H. H. (2005). Crop systems dynamics: an ecophysiological simulation model for genotype-
1361 by-environment interactions. Wageningen: Wageningen Academic Publishers.

1362 Zhang, K., Burns, I. G., Broadley, M. R., & Turner, M. (2003). Developing a dynamic model for glasshouse
1363 lettuce growth and nitrate accumulation. Paper presented at the International Workshop on Models for
1364 Plant Growth and Control of Product Quality in Horticultural Production.
1365 <https://doi.org/10.17660/ActaHortic.2004.654.6>

1366 Zhang, X., Wang, Y., Huang, G., Feng, F., Liu, X., Guo, R., . . . Mei, X. (2020). Atmospheric humidity and
1367 genotype are key determinants of the diurnal stomatal conductance pattern. *Journal of Agronomy and
1368 Crop Science*, 206(2), 161-168. <https://doi.org/10.1111/jac.12375>

1369